1992-03

Tests of a convective cloud model with soundings during the TCM-90 field experiment.

Yin, Tzyh-Chyang

Monterey, California. Naval Postgraduate School

NAVAL POSTGRADUATE SCHOOL

Monterey, California

THESIS

TESTS OF A CONVECTIVE CLOUD MODEL WITH SOUNDINGS DURING THE TCM-90 FIELD EXPERIMENT

by

Yin Tzyh-Chyang

March, 1992

Thesis Advisor: Pe-Cheng Chu

Approved for public release; distribution is unlimited

SECURITY CLASSIFICATION OF THIS PAGE

REPORT DOCUMENTATION PAGE

1a. REPORT SECURITY CLASSIFICATION Unclassified	1b. RESTRICTIVE MARKINGS
2a. SECURITY CLASSIFICATION AUTHORITY	3. DISTRIBUTION/AVAILABILITY OF REPORT Approved for public release;Distribution is unlimited
2b. DECLASSIFICATION/DOWNGRADING SCHEDULE	
4. PERFORMING ORGANIZATION REPORT NUMBER(S)	5. MONITORING ORGANIZATION REPORT NUMBER(S)

6a. NAME OF PERFORMING ORGANIZATION Naval Postgraduate School	6b. OFFICE SYMBOL *(If applicable)* MR	7a. NAME OF MONITORING ORGANIZATION Naval Postgraduate School	
6c. ADDRESS (*City, State, and ZIP Code*) Monterey, CA 93943-5000		7b. ADDRESS (*City, State, and ZIP Code*) Monterey, CA 93943-5000	
8a. NAME OF FUNDING/SPONSORING ORGANIZATION	8b. OFFICE SYMBOL *(If applicable)*	9. PROCUREMENT INSTRUMENT IDENTIFICATION NUMBER	
8c. ADDRESS (*City, State, and ZIP Code*)		10. SOURCE OF FUNDING NUMBERS	
		Program Element No	Project No / Task No / Work Unit Accession Number

11. TITLE (*Include Security Classification*)
TESTS OF A CONVECTIVE CLOUD MODEL WITH SOUNDINGS DURING THE TCM-90 FIELD EXPERIMENT

12. PERSONAL AUTHOR(S)
Yin Tzyh-Chyang

13a. TYPE OF REPORT	13b. TIME COVERED	14. DATE OF REPORT (*year, month, day*)	15. PAGE COUNT
Master's Thesis	From To	March 1992	75

16. SUPPLEMENTARY NOTATION
The views expressed in this thesis are those of the author and do not reflect the official policy or position of the Department of Defense or the U.S. Government.

17. COSATI CODES			18. SUBJECT TERMS (*continue on reverse if necessary and identify by block number*)
FIELD	GROUP	SUBGROUP	Cumulus Parameterization, Radiative-Convective Equilibrium Simulation, Precipitation rates

19. ABSTRACT (*continue on reverse if necessary and identify by block number*)

A new proposed scheme for representing cumulus convection in a large-scale numerical model has been tested using the dataset collected during the Tropical Cyclone Motion (TCM-90) field experiment. This new scheme by K. Emanuel incorporated some modifications, which are based on recent observations of convective clouds, and showed much of the vertical transport of convective clouds was accomplished by subcloud-scale drafts rather than by the clouds themselves. These small-scale drafts were idealized and regarded as the fundamental agents of the convective transport. The input to the idealized model of subcloud-scale updrafts and downdrafts is the one-dimensional arrays of temperature and mixing ratio as a function of pressure, and the output is the tendency of potential temperature and the tendency of mixing ratio as well as the rate of convective precipitation.

In this test, 46 dropwindsondes from the TCM-90 dataset with a vertical resolution of 10 mb were chosen as inputs. The convection scheme is integrated in time to investigate the outputs of precipitation rates. The model was forced with constant radiative cooling, convective heating/and moistening calculated from model and surface fluxes in all cases . We conclude that this new modified convective scheme predicts quite reasonable precipitation rates in the regions beyond 4 degree latitude radius, but not near the center (too small) of Supertyphoon Flo on 16, 17 and 18 September 1990.

20. DISTRIBUTION/AVAILABILITY OF ABSTRACT	21. ABSTRACT SECURITY CLASSIFICATION	
☒ SAME AS REPORT ☐ DTIC USERS	Unclassified	
22a. NAME OF RESPONSIBLE INDIVIDUAL Pe-Cheng Chu	22b. TELEPHONE (*Include Area code*) (408) 646-3257	22c. OFFICE SYMBOL OC/Chu

DD FORM 1473, 84 MAR 83 APR edition may be used until exhausted
All other editions are obsolete

SECURITY CLASSIFICATION OF THIS PAGE
Unclassified

Approved for public release; distribution is unlimited.

Tests of a Convective Cloud Model with Soundings During the TCM-90 Field Experiment

by

Yin Tzyh-Chyang
Lieutenant Commander, Taiwan, R.O.C. Navy
B.S., Chung-Cheng Institute of Technology,
Taiwan, R.O.C., 1979

Submitted in partial fulfillment
of the requirements for the degree of

MASTER OF SCIENCE IN METEOROLOGY

from the
NAVAL POSTGRADUATE SCHOOL

March 1992

ABSTRACT

A new proposed scheme for representing cumulus convection in a large-scale numerical model has been tested using the dataset collected during the Tropical Cyclone Motion (**TCM-90**) field experiment. This new scheme incorporated some modifications by K. Emanuel, which are based on recent observations of convective clouds, and showed much of the vertical transport of convective clouds was accomplished by subcloud-scale drafts rather than by the clouds themselves. These small-scale drafts were idealized and regarded as the fundamental agents of the convective transport. The input to the idealized model of subcloud-scale updrafts and downdrafts is the one-dimensional arrays of temperature and mixing ratio as a function of pressure, and the output is the tendency of potential temperature and the tendency of mixing ratio as well as the rate of convective precipitation.

In this test, 46 dropwindsondes from the **TCM-90** dataset with a vertical resolution of 10 mb were chosen as inputs. The convection scheme is integrated in time to investigate the outputs of precipitation rates. The model was forced with constant radiative cooling, convective heating/and moistening calculated from model and surface fluxes in all cases. We conclude that this new modified convective scheme predicts quite reasonable precipitation rates in the regions beyond 4° latitude radius, but not near the center (too small) of **Supertyphoon Flo** on 16, 17 and 18 September 1990.

C.1

TABLE OF CONTENTS

I. INTRODUCTION 1

A. CONVECTIVE SCHEMES IN NUMERICAL MODELS 1

B. PURPOSE OF THE STUDY 4

II. OBSERVATIONAL BASIS AND ANALYSIS 7

A. MIXING IN CLOUDS 7

B. PRECIPITATION-DRIVEN DOWNDRAFTS 9

III. MODEL THEORY AND EQUATIONS 11

A. THE MODEL DESCRIPTION 11

B. MAJOR MODEL EQUATIONS 14

1. The Undiluted Updraft Mass Fluxes 14

2. The Fluxes of Saturated Updrafts and Downdrafts 15

3. Unsaturated Downdrafts 16

4. Convective Heating and Moistening 17

C. CLOSURE PARAMETERS OF THE MODEL: ϵ^i , $\sigma_s{}^i$, σ_d 19

IV. DATA COLLECTION AND HANDLING PROCEDURES 21

A. DATA COLLECTION 21

B. DATA PREPARATION 22

C. DATA PROCESSING 28

V. RADIATIVE-CONVECTIVE EQUILIBRIUM SIMULATION 30

A. USING A PARTICULAR SOUNDING FROM THE TROPICAL WESTERN PACIFIC 30

B. USING TCM-90 DROPWINDSONDE DATA 41

C. HORIZONTAL DISTRIBUTION OF PRECIPITATION PREDICTED BY THE MODEL 46

D. SENSITIVITY SIMULATIONS 54

1. Case A 54

2. Case B 55

3. Case C 56

4. Case D 57

5. Case E 58

VI. CONCLUSIONS 62

APPENDIX A. SUBROUTINE ESAT 64

APPENDIX B. THERMODYNAMIC CONSTANTS AND EQUATIONS 65

REFERENCES 66

INITIAL DISTRIBUTION LIST 68

I. INTRODUCTION

A. CONVECTIVE SCHEMES IN NUMERICAL MODELS

Because of the importance of convection to the evolution of the larger scale system, considerable effort has been directed toward developing methods for representing the net effect of the many short-lived convective cells on the thermodynamic, moisture and momentum structures of the environment. From a modeling point of view, the cumulus parameterization schemes may be divided into two main classes: (i) convective adjustment; and (ii) cloud-model schemes.

In the convective-adjustment type, also referred to as moist convective adjustment, the moisture and thermodynamic fields are simply adjusted toward a moist neutral state to eliminate superadiabatic lapse rates and supersaturation in which the equivalent potential temperature is constant with height. When the atmosphere becomes superadiabatic, it is adjusted back to its adiabatic value. These bulk-adjustment schemes contribute little to the understanding of how the convection and the large scale circulation interact, and are probably not capable of representing the variety of subtle feedbacks between the convection and the large-scale structure of the environment. When the atmosphere is unstable and moist convection with condensation takes place, the processes are more complex and the problem is far more involved. In addition, it is not generally agreed that the adjusted state is convectively neutral.

The convective-adjustment schemes are not representations of the ensemble effects of unresolved clouds, but rather represent convective adjustments within explicitly resolved clouds. As pointed out by Emanuel (1991), these adjustments prevent the explicit clouds from being locally unstable to small vertical displacements within the clouds. The final state is assumed to be saturated in the fraction of grid box assumed to contain cloud, and all condensed water is removed as precipitation. It is important to note that grid-scale clouds are being formed in the large-scale model, and the convective adjustment scheme only ensures that they are internally stable.

The second type of cumulus parameterization scheme includes the effect of subgrid-scale penetrative convection on the large-scale equations through solution of a model of the clouds. Once the cloud distribution and the cloud properties (i.e., temperature, humidity, momentum, etc) are determined, their effects on their environment may be computed in the large-scale equations. Examples of this type are given by Kuo (1965, 1974), Arakawa and Schubert (1974), an extension of the Kuo scheme by Anthes (1976), and Betts (1986). Although these schemes are capable of representing more of the details of the cloud-environment interactions, there exist some drawbacks and unrealistic aspects to such schemes. As pointed out by Emanuel (1991), the Betts scheme is a proper representation of the ensemble effects of clouds only when the large scale is unstable to parcel ascent. Since the imposed profiles effectively determine both the vertically-integrated heating (precipitation) and the profile of moistening, the predicted structures in the temperature and water vapor profiles are severely limited.

In the Kuo scheme (1965, 1974), which is applied in many models, the cumulus clouds are assumed to dissolve immediately by mixing with the environmental air, and result in changes of the large-scale temperature and humidity distribution. Kuo assumes that the vertically-integrated heating is equal to the explicitly resolved convergence of water vapor. Some unrealistic aspects in Kuo's scheme are the vertical partitioning of the cloud-scale heating and the determination of the percent area covered by cumulus convection. Emanuel (1991) pointed out that in some conditions conditional instability can accumulate in the absence of moisture convergence and evaporation, and result in larger convective available potential energy than normally expected.

The Arakawa and Schubert scheme (1974) is based on a theory of interaction between a cumulus ensemble and the large-scale environment. As in other schemes, the cumuli modify the large-scale temperature and humidity through detrainment of saturated air and condensation products and by the subsidence induced by the convection. One of the important innovations is the partitioning of cumulus ensemble into subensembles, or cloud types, each characterized by a unique fractional entrainment rate. This scheme relates the distribution of the vertical mass flux at the cloud base into the subensembles by the large-scale dynamic and physical processes. The fundamental assumption is that the generation of moist convective instability by large-scale processes is in near-equilibrium with the destruction of this instability by the vertical transport of heat and moisture within the clouds. Lord (1982) showed the scheme produces too much warming and drying at low levels. The main drawback of the elegant scheme of Arakawa and Schubert is that it contains no downdrafts. As pointed out by Emanuel (1991), the

Arakawa-Schubert scheme relies on an entraining plume model and it can not be expected to handle episodes of stored-energy convection.

The main problems in representing cumulus convection are to account for the redistribution of water, determine how much condensed water ultimately falls out as rain (which governs the net heating), and specify the vertical distribution of moistening. These moisture processes depend on the details of cloud dynamical and microphysical parameters, as pointed out by Ooyama (1971). Many convective schemes used in large-scale models avoid addressing the details of such processes by making sweeping assumptions about the distributions of moistening and/or heating by clouds. Moreover, Emanuel (1991) pointed out that the vertical distribution of heating is a poor validation field for convective schemes because it is determined almost entirely by the large-scale profile of adiabatic and radiative cooling, which together balance almost all of the convective heating.

B. PURPOSE OF THE STUDY

A new convective scheme proposed by Emanuel (1991) based on the physics and microphysics of cloud process will be applied in one-dimensional radiative-moist convective equilibrium experiments using a particular sounding from the tropical western Pacific. This scheme produced reasonable profiles of buoyancy and relative humidity. In this thesis, this scheme will be used to predict the precipitation rates in **Supertyphoon Flo** on 16,17 and 18 September.

A similar version of the convective model has been tested in the European Center for Medium-range Weather Forecasts model and appeared to work well. This new version includes several important modifications suggested by Emanuel (1991). The most important modification was required because the vertically-integrated moisture sink was not consistent with the integrated heat source, in that the heat capacity of condensed water was being accounted for in the ascent but not in falling precipitation. The latter had already been added to the heating term. Because of the complex mixing processes in this scheme, the energy balance is still not exact, but it is good to within 1% of the latent heating term.

The main purposes of this study are to investigate the properties of the new proposed model by Emanuel (1991) and to use special dropwindsondes to predict the precipitation of the **Supertyphoon Flo** in the western North Pacific on 16, 17 and 18 September 1990. The dropwindsonde data consist of pressure, temperature and dew-point temperature with a high vertical resolution of 10 mb, and were obtained between 5°N and 40°N, 105°E and 150°E in the western North Pacific.

The Tropical Cyclone Motion (**TCM-90**) field experiment in the western North Pacific area was carried out during August/September 1990 by the United States Office of Naval Research. Separate (but coordinated) experiments were carried out by the Economic and Social Commission for Asia and the Pacific/World Meteorological Organization (**ESCAP/WMO**) Typhoon Committee, by the Soviet Union and by Taiwan, Republic of China. The combined observations from these experiments have produced

a comprehensive and the best-ever datasets to study tropical cyclones in the western North Pacific (Elsberry 1990; Elsberry et al. 1990; Harr et al. 1991).

Chapter II reviews the recent observational basis for analysis of convective clouds. Chapter III describes the mathematical basis of the model and the physical interpretations and assumptions. Chapter IV describes the data collection and handling. Chapter V shows the results of the controlled model simulation and from the **TCM-90** data, and discusses the differences of the results. Finally, Chapter VI states the conclusions from this study.

II. OBSERVATIONAL BASIS AND ANALYSIS

A. MIXING IN CLOUDS

It has long been realized that mixing must take place between a growing cumulus cloud and its environment. This is apparent from our understanding of turbulent processes as well as from observations of the internal properties of clouds. Entrainment in cumulus clouds is often thought to resemble entrainment in plumes (Stommel 1947). The clouds are thought to entrain environmental air from the sides and carry it along with the updraft, which is therefore expected to contain environmental air entrained from below.

A different entrainment mechanism has been proposed by Squires (1958a) who showed that cloud air mixed with the (dry and cool) environmental air at the cloud top undergoes evaporative cooling (i.e., the cloud water evaporates and cools the mixture). The mixed air can penetrate and dilute the cloud air below (or the updraft air), and lead to a phenomenon called penetrative downdrafts. Observations of the structure of cumulus clouds by Squires (1958b) suggested that this might be the primary mode of mixing in cumuli. In a review of turbulence and mixing processes in cloud dynamics, Telford (1975) suggests that penetrative downdrafts are the dominant mixing process in clouds.

Paluch (1979) presented the first concrete observational evidence of the occurrence of penetrative downdrafts. She used the conserved thermodynamic variables θ_q (the wet equivalent potential temperature) and Q_{total} (the total water mixing ratio) to deduce the

mixed cloud air stability in Colorado cumuli. In the case of entrainment of dry air into a cloud, the mixed air first becomes negatively buoyant because of evaporative cooling, and regains buoyancy only later when it is diluted through further mixing with cloud air. Supporting evidence was provided by Emanuel (1981), who pointed out that these unsaturated downdrafts may penetrate deep into clouds, with velocities comparable to or stronger than those associated with the buoyant updrafts. He also suggests that such downdrafts are fundamentally distinct from classical dry or moist convection in that they rely on turbulent mixing to provide simultaneously the liquid water and dry air necessary for evaporative cooling. This phenomenon is therefore peculiar to clouds and provides a mechanism for an alternate model of cumulus cloud dilution, namely, vertical mixing.

Telford (1975) found that the vertical distribution of liquid water in mixed parcels that had reached their level of neutral buoyancy agreed well with profiles of liquid water measured in cumulus clouds. Raymond (1979) further found similar results in a dynamic model incorporating the same ideas. Unfortunately, Telford (1975) assumed that environmental air enters only at cloud top, whereas recent evidence indicates that this may be an oversimplification. Blyth et al. (1986) used Paluch's (1979) method to show that environmental air can enter a cloud at all levels. Most recently, Raga et al. (1990) studied the cumulus clouds off the coast of Hawaii and showed that entrainment into the clouds occurs at all levels. Since evaporative cooling does play a role in the descent of cloud top air to the bottom of the inversion, this implies penetrative downdrafts near the cloud top.

Using cloud observations to study an entraining plume model, Warner (1970) found that the simple lateral entrainment model can not simultaneously predict observed values of liquid water content and cloud depth. Observations of cumulus clouds by recent researchers suggest that the lateral entrainments occur as well as the vertical entrainments. However, the relative importance of these two entrainment mechanisms has not been completely established.

The dominant role of penetrative downdrafts in cumulus dynamics, which is implied by observations, is the basis of the present work. Emanuel (1981, 1991) stated that the failure to account for the presence of penetrative downdrafts in most cumulus clouds may lead to a serious misrepresentation of their dynamics. Therefore, it is instructive to consider the case of a two-step process in which air parcels from a well-mixed subcloud layer are moist adiabatically lifted to a prescribed level at which they attain a state of neutral buoyancy with respect to their environment, and then are subjected to the action of penetrative downdrafts.

B. PRECIPITATION-DRIVEN DOWNDRAFTS

In convective regions of the atmosphere, a strong upward decrease of θ_e (equivalent potential temperature) and q (mixing ratio) is usually found in the middle level. This low θ_e in the middle level creates a large potential for downdrafts driven by the evaporation of precipitation that falls into the dry air from a cloud. Precipitation falling from an upper cloud layer and evaporating below can warm the upper layer and cool the lower one. Thus, air in a precipitation-driven penetrative downdrafts can change its θ_v (virtual

potential temperature) equilibrium level and bring down air from above with relatively low θ_e to give the local q and θ_e minima at low level (Betts 1986). Such downdraft-induced cooling plays an important role in cloud dynamics. It tends to cancel the heating by convective towers and the total heating at lower levels (Houze 1989). In particular, its propensity to mix with the environment and sink as a result of evaporative cooling has a major effect on cumulus mass flux profiles. As pointed out by Emanuel (1981), these downdrafts constitute an important way by which convection stabilizes the atmosphere both by heating the free atmosphere and drying out the subcloud layer. Therefore, a successful representation of convection in a numerical model must take into account for the effects of unsaturated downdrafts.

III. MODEL THEORY AND EQUATIONS

A. THE MODEL DESCRIPTION

In view of the observations discussed in the previous section, Emanuel (1991) constructed a moist convective transport model for large-scale numerical simulations. The fundamental entities of the vertical transport are accomplished by subcloud-scale updrafts and downdrafts rather than by the clouds, as in most existing parameterizations. The idealization of the convective process formulated by Emanuel (Fig. 1) is based on the models of Raymond and Blyth (1986) and Telford (1975).

The transport by these subcloud-scale (i.e., small-scale) drafts is idealized as follows. The level of cloud base (**ICB**) and the first level of neutral buoyancy (**INB**) for the undiluted, reversible ascent air from near the surface are first determined from the sounding. Here **ICB** is defined the first level above the lifted condensation and **INB** is the first model level above the parcel's level of neutral buoyancy. If the first **INB** is at an altitude higher than the **ICB**, convection is assumed to occur. Thus, air from the subcloud layer is lifted to an arbitrary level i between **ICB** and **INB** for undiluted air. A specified fraction, ϵ^i, of the condensed water will be converted into precipitation, which falls and completely or partially evaporates in a single unsaturated downdraft. The remaining cloudy air is mixed with its environment at level i. For the sake of simplicity, Emanuel (1991) assumed an equal probability distribution of the mixing fraction σ^i,

following Raymond and Blyth (1986). Each mixture then ascends or descends to its new level of neutral buoyancy according to its buoyancy.

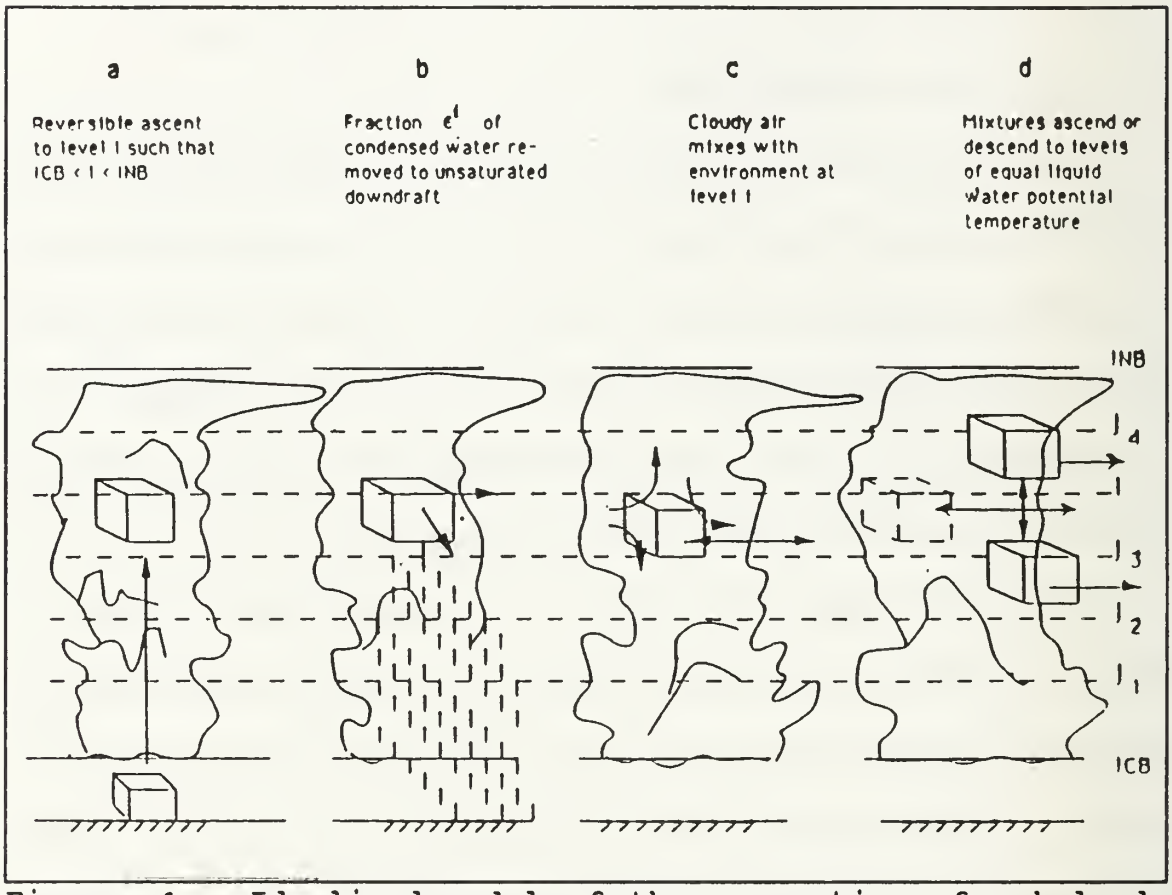

Figure 1. Idealized model of the convection of subcloud-scale parcels from Emanuel (1991).

A problem with this hypothesis, as pointed out by Taylor and Baker (1991) and Emanuel (1991), is that cloudy air detrained at its level of neutral buoyancy will usually become negatively buoyant on mixing with its new environment. It seems likely that mixing will occur again and the new mixtures will once again proceed to their new levels of neutral buoyancy. Thus, this process may involve many mixing events, as shown in Fig. 2.

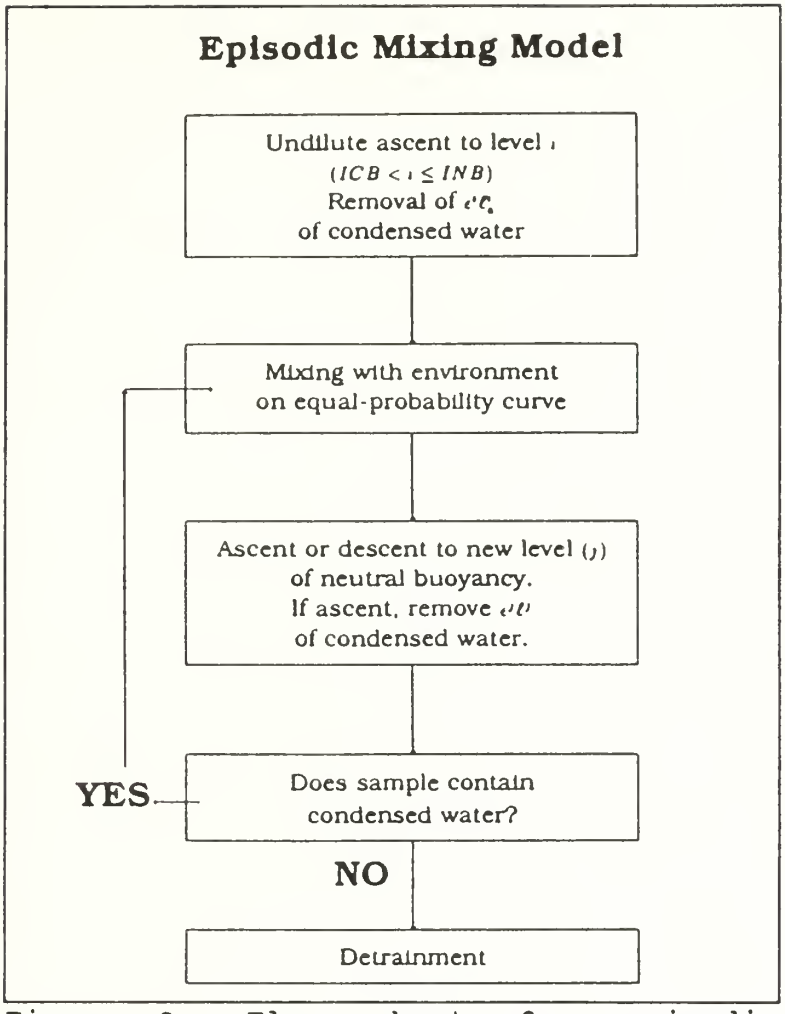

Figure 2. Flow chart for episodic mixing model from Emanuel (1991).

It is necessary to truncate this mixing process at some level for practical application. Emanuel (1991) suggests that the mixture detrains only at levels where further mixing with the environment will result in neutral buoyancy. This is equivalent to assuming that the mixtures detrain at levels at which their liquid water potential temperature (θ_l^{ij}) equals the potential temperature of the environment (θ_j), i.e., without further precipitation formation, for $\theta_l^{ij} = \theta^j$. While the assumption of detrainment at

levels of equal θ_l is somewhat unphysical, it avoids the problem of detraining air that would become negatively buoyant on further mixing. In his control simulation, Emanuel (1991) showed that none of the detraining mixed air contained any condensed water, since descending air will usually have small or zero condensed water content, while ascending air is assumed to have more condensed water removed by precipitation. Therefore, he claims that the proposed method appears to be the best way to truncate a series of discrete mixing events.

B. MAJOR MODEL EQUATIONS

1. The Undiluted Updraft Mass Fluxes

The updraft mass fluxes M^i are represented as vertical velocities W^i multiplied by fractional areas σ^i and the air density at level i, ρ^i. Thus,

$$M^i = \sigma^i \rho^i W^i \quad , \tag{3-1}$$

where σ^i is determined in such a way as to drive the mass fluxes toward a state of quasi-equilibrium with the large-scale forcing. The vertical velocities are determined by the amount of the subcloud parcel's convective available potential energy (**CAPE**) for undiluted ascent to level i, i.e.,

$$W^i = \sqrt{2 CAPE^i} \quad . \tag{3-2}$$

2. The Fluxes of Saturated Updrafts and Downdrafts

The mass flux from level i to level j of a particular mixture $MENT^{ij}$ is given by

$$MENT^{ij} = \frac{M^i \left(|\sigma^{ij+1} - \sigma^{ij}| + |\sigma^{ij} - \sigma^{ij-1}| \right)}{(1-\sigma^{ij}) \sum_{j=ICB-1}^{INB} \left[|\sigma^{ij+1} - \sigma^{ij}| + |\sigma^{ij} - \sigma^{ij-1}| \right]} \quad , \qquad (3-3)$$

provided $0 < \sigma^{ij} < 1$. Here, M^i is the updraft mass flux and σ^{ij} is the fraction of environmental air in the mixture, which can be determined by

$$\sigma^{ij} = \frac{\theta^j - \theta_{lp}^{ij}}{\theta_l^{ij} - \theta_{lp}^{ij}} \quad , \qquad (3-4)$$

where θ_l^{ij} is the θ_l (liquid water potential temperature) of the environment after being lifted to level j and θ_{lp}^{ij} is the θ_l of subcloud air after first being lifted to level i, depleted of water by precipitation, and then lifted to level j with further removal of precipitation if $j > i$. The requirement is that the θ_l of the mixture displaced to level j equals the θ_l of the environment at level j, assuming the environment has no condensed water.

A total water content associated with each entrained air flux $MENT^{ij}$ will be given by

$$QENT^{ij} = \sigma^{ij} + (1 - \sigma^{ij}) (r^i - \epsilon^i l_a^i) \quad , \qquad (3-5)$$

where r^i is the environmental mixing ratio at level i and l_a^i is the adiabatic water content at that level.

Thus, the fluxes $MENT^{ij}$ should be unique functions of the flux M^i and the environmental moisture and temperature distributions.

3. Unsaturated Downdrafts

These unsaturated downdrafts are driven by the evaporation of precipitation between the cloud base (**ICB**) and the cloud top (**INB**), which includes updrafts of mixed as well as undiluted air. In this scheme, the precipitation content of the unsaturated downdraft is found by integrating the conservation equation

$$\frac{d}{dp}(\omega_T l_p \sigma_d)^i = \frac{g}{\Delta p}\epsilon^i l_a^i M^i + \frac{g}{\Delta p}\epsilon^i \sum_{j=1}^{i-1} [QENT^{ji} - r^{*i}]\, MENT^{ji}$$

$$- \sigma_d \sigma_s^i E^i \quad , \qquad (3\text{-}6)$$

where ω_T is the terminal "omega" of the precipitation, l_p is the precipitation mixing ratio, σ_d is the fractional area covered by the downdraft, ΔP is the difference in pressure between two levels centered at i, r^{*i} is the saturation mixing ratio at level i and E^i is the rate of evaporation of precipitation. The parameter σ_s^i, where $0 \leq \sigma_s \leq 1$, is approximately the fraction of precipitation that falls through the environment rather than through the cloud. If $\sigma_s^i = 1$ for $i <$ **ICB**, then all precipitation is subject to evaporation below the cloud base.

The first and second terms in (3-6) are the rate of detrainment of precipitation from updrafts ending at level i, and the third term is the loss of precipitation by evaporation. The surface precipitation rate, P, is then given by

$$P = (g^{-1}\omega_T l_p \sigma_d)^{i=0} \quad . \tag{3-7}$$

The ω_T and E are in general functions of the precipitation mixing ratio (l_p) and the thermodynamic properties of the environment.

4. Convective Heating and Moistening

The convective forcing of potential temperature results from condensation, evaporation and the fluxes of heat by updrafts and downdrafts

$$\left(\frac{\partial\theta}{\partial t}\right)^i = -g\left(\frac{\partial\theta}{\partial p}\right)^i \sum_{n=i}^{INB} \underbrace{\left(M^n + \sum_{k=1}^{i-1} (MENT^{k,n} - MENT^{n,k})\right)}_{(i)} + \underbrace{\frac{g}{\theta^i}(\theta_{lc}^i - \theta^i)\frac{M^i}{\Delta p}\delta^i}_{(ii)}$$

$$\underbrace{- \frac{g}{\theta^i}\frac{\partial}{\partial p}[M_p^i(\theta_p^i - \theta^i)]}_{(iii)} \underbrace{- \theta^i \frac{L_v}{C_p T^i}\sigma_d \sigma_s^i E^i}_{(iv)} \quad , \tag{3-8}$$

where θ_{lc}^i is the liquid water potential temperature of the subcloud air lifted to level i after it has been depleted of precipitation, θ_{pi} is the potential temperature of the plume (unsaturated downdraft) and

$$\delta^i = \begin{cases} 1 & if\ N^i = 0 \\ 0 & otherwise \end{cases} \tag{3-9}$$

where N^i is the number of drafts entraining at level i. The total convective tendency of potential temperature is the sum of the effect of in-cloud drafts, which are terms (i) and (ii) in (3-8), and the effects of unsaturated downdrafts, which are terms (iii) and (iv).

The total convective moistening due to the various updrafts and downdrafts and the evaporation of precipitation is given by

$$\left(\frac{\partial r}{\partial t}\right)^i = -g\left(\frac{\partial r}{\partial p}\right)^i \sum_{n=i}^{INB} \left(M^n + \sum_{k=1}^{i-1} \underbrace{(MENT^{k,n} - MENT^{n,k})}_{(i)}\right)$$

$$+ \frac{g}{\Delta p} \sum_{n=1}^{INB} \underbrace{MENT^{n,i}(QENT^{n,i} - \epsilon^i l^{n,i} - r^i)}_{(ii)} + \frac{g}{\Delta p} \underbrace{M^i \delta^i (r^1 - \epsilon^i l_a^i - r^i)}_{(iii)}$$

$$- g\frac{\partial}{\partial p} \underbrace{[M_p^i (r_p^i - r^i)]}_{(iv)} + \underbrace{\sigma_d \sigma_s^i E^i}_{(v)} \quad , \qquad (3\text{-}10)$$

where $l^{n,i}$ is the adiabatic condensed water content of the buoyancy-sorting updraft and r_p^i is the vapor mixing ratio of the downdraft at level i. Thus, the water vapor content is affected by

(i) vertical advection of environmental water vapor by compensating updrafts;

(ii) vertical advection of environmental water vapor by compensating downdrafts;

(iii) detrainment of water substance (including condensate) at the termination of in-cloud drafts;

(iv) downward advection of dry air by unsaturated downdrafts; and

(v) evaporation of falling precipitation.

C. CLOSURE PARAMETERS OF THE MODEL: ϵ^i , σ_s^i , σ_d

Emanuel (1991) pointed out that the main closure parameters in this scheme are the parcel precipitation efficiencies, ϵ^i, and the fraction of precipitation that falls through unsaturated environment, σ_s^i. The vertical profiles of relative humidity are quite sensitive to these parameters, just as nature must be sensitive to the details of how condensed water is converted into precipitation. Specification of these parameters determines the vertical profiles of heating and moistening by cloud dynamical and microphysical processes. In particular, they represent the physical processes responsible for determining how much condensed water reevaporates, which moistens and cools the air, and how much falls out of the system, which leads to warming and drying.

The ϵ^i values determine the fraction of condensed water in an individual updraft lifted to level i that is converted to precipitation. Qualitatively, one may expect that ϵ^i increases from zero near the cloud base to close to one in the upper troposphere. Following Emanuel (1991), ϵ^i are specified according to

$$\epsilon^i = \begin{cases} 0 & p^{ICB} - p^i < p^c \\ \dfrac{p^{ICB} - p^i < p^c}{p^t - p^c} & p^c < p^{ICB} - p^i < p^t \\ 1 & p^{ICB} - p^i > p^t \end{cases} , \qquad (3\text{-}11)$$

where p^c (=150 mb) is a critical cloud depth, which means the precipitation efficiency is assumed to be zero for all shallower clouds. Similarly, p' (=500 mb) is also a critical cloud depth, such that all condensate is converted to precipitation for cloud depths exceeding 500 mb. In between, the precipitation efficiency varies linearly.

The σ_s^i value determines how much precipitation falls back through cloudy air as opposed to falling through environmental (clear) air, which is highly dependent on the exact configuration of the cloud. Therefore, setting σ_s^i is more problematic. To avoid a more involved approach to the problem, Emanuel specifies a profile of σ_s^i by letting

$$\sigma_s^i = \begin{cases} 0.15 & i \geq ICB \\ 1.0 & i < ICB \end{cases} \quad . \qquad (3\text{-}12)$$

As pointed out by Emanuel in his simulation, there is a weak dependence on σ_d which determines the fractional area covered by the precipitating downdraft. Emanuel chooses a specification of σ_d that yields reasonable values of the precipitation content l_p^i by setting σ_d=0.01. In addition, the rate of approach of the mass fluxes to quasi-equilibrium is controlled by the parameters α and β. Their standard values are defined to 1.0.

Many considerations and assumptions have being taken into account in this scheme. The interested reader is referred to the original Emanuel (1991) article for the detailed development.

IV. DATA COLLECTION AND HANDLING PROCEDURES

A. DATA COLLECTION

The primary data set comes from dropwindsondes collected during the TCM-90 field experiment (Elsberry et al. 1990; Harr et al. 1991). Although the main purpose for gathering these observations was to improve basic understanding of tropical cyclone motion, they also provide thermodynamic data with a high vertical resolution of 10 mb. Figure 3 shows the approximate flight paths for the dropwindsonde missions.

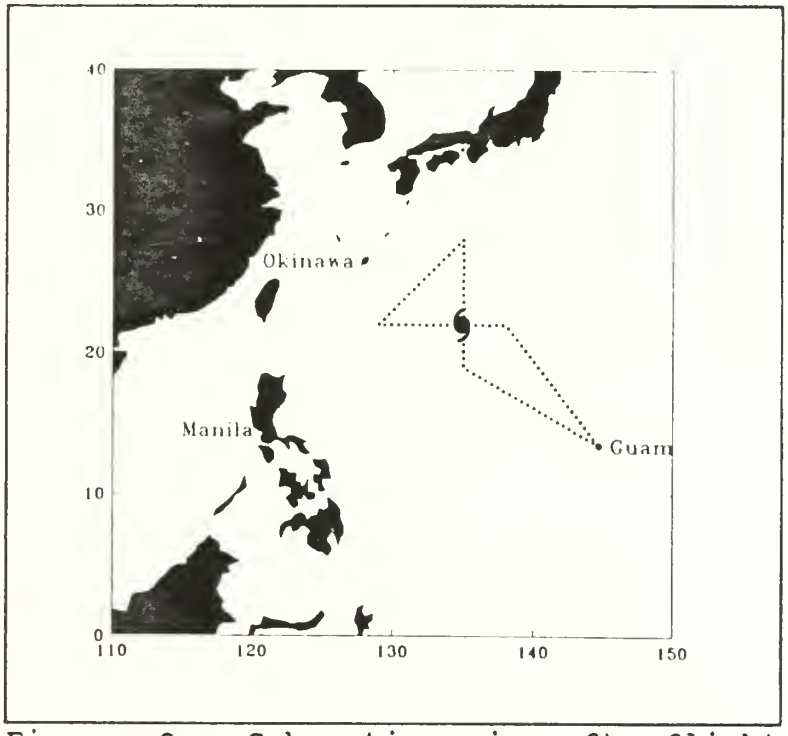

Figure 3. Schematic aircraft flight track from Elsberry (1990).

The **TCM-90** data base is constructed from a combination of: (i) Real-time data were collected during the field phases of the four concurrent (e.g., the United States, USSR, Typhoon Committee, and Taiwan) tropical cyclone experiments; and (ii) Delayed data collected after the field experiment phase. Some observations were only available as delayed data (e.g., nontransmitted experimental data, post-processed data, etc.). For example, these dropwindsonde reports were not available in real time because the aircraft had a limited communication capability. All of the delayed and real-time data sets were combined and stored at the Data Integration Center at the Naval Postgraduate School under the direction of Patrick Harr and Tamar Neta. The **"raw"** data are the real-time, delayed, and postexperiment data from the instrument operators and specialized centers, or from cooperating experiments. Quality control procedures have only been applied to the real-time data (Harr et al. 1991). The screened data in the **FGGE Level II** format are now available for members and non-members. For many users, the raw or screened data will be adequate for research or prediction studies.

B. DATA PREPARATION

There are 73 soundings from the three **Supertyphoon Flo** flights for 16, 17 and 18 September 1990. First, soundings with major data gaps were simply omitted. Although the dropwindsondes in the **FGGE** format do not include surface data, data usually were available at 1000 mb. Some subjective interpolation of missing data had been performed because missing data were often found at the top or bottom of the descent. After these examinations, there were 46 dropwindsondes left for this study, as

listed in Table I. The best-track data of the **Supertyphoon Flo** for 16, 17 and 18 September are listed in Table II. The dropwindsonde locations relative to the position of the **Supertyphoon Flo are also** plotted for each day, as illustrated in Figs. 4a-c.

TABLE I. DROPWINDSONDE STATION ID, LATITUDE AND LONGITUDE FOR THE THREE SUPERTYPHOON FLO MISSIONS.

TIME	06 UTC 16 Sept.		06 UTC 17 Sept.		06 UTC 18 Sept.	
STID	Lat.	Long.	Lat.	Long.	Lat.	Long.
DC01	25.77	128.61	15.11	142.92	16.51	143.94
DC02	23.95	127.88	16.24	141.39	17.81	143.96
DC03	24.05	129.33	18.70	138.12	20.45	143.96
DC04	23.36	131.82	19.49	137.05	22.50	143.49
DC05	23.54	133.02	22.99	134.75	22.54	142.07
DC06	21.99	132.77	22.93	133.22	22.54	137.54
DC07	22.01	131.24	22.91	130.85	22.93	135.38
DC08	25.31	132.07	29.03	128.44	25.10	137.26
DC09	23.91	133.05	29.97	128.80	26.11	135.17
DC10	22.70	133.77	29.11	132.71	27.05	138.65
DC11	21.37	134.28	26.96	135.17	27.01	135.35
DC12	20.51	135.67	25.98	136.24	27.00	133.50
DC13	19.17	136.73	23.41	137.84	29.49	127.99
DC14	18.00	139.09	22.08	138.50		
DC15	16.20	141.44	20.18	139.17		
DC16	15.06	142.97	18.74	139.72		
DC17			16.89	140.42		

TABLE II. BEST-TRACK POSITIONS AT 06 UTC OF SUPERTYPHOON FLO DURING THE FIELD EXPERIMENT PHASE OF TCM-90.

Date	Latitude	Longitude	Intensity(kts)
16 September	23.30N	130.70E	115
17 September	25.60N	128.90E	145
18 September	28.40N	130.20E	115

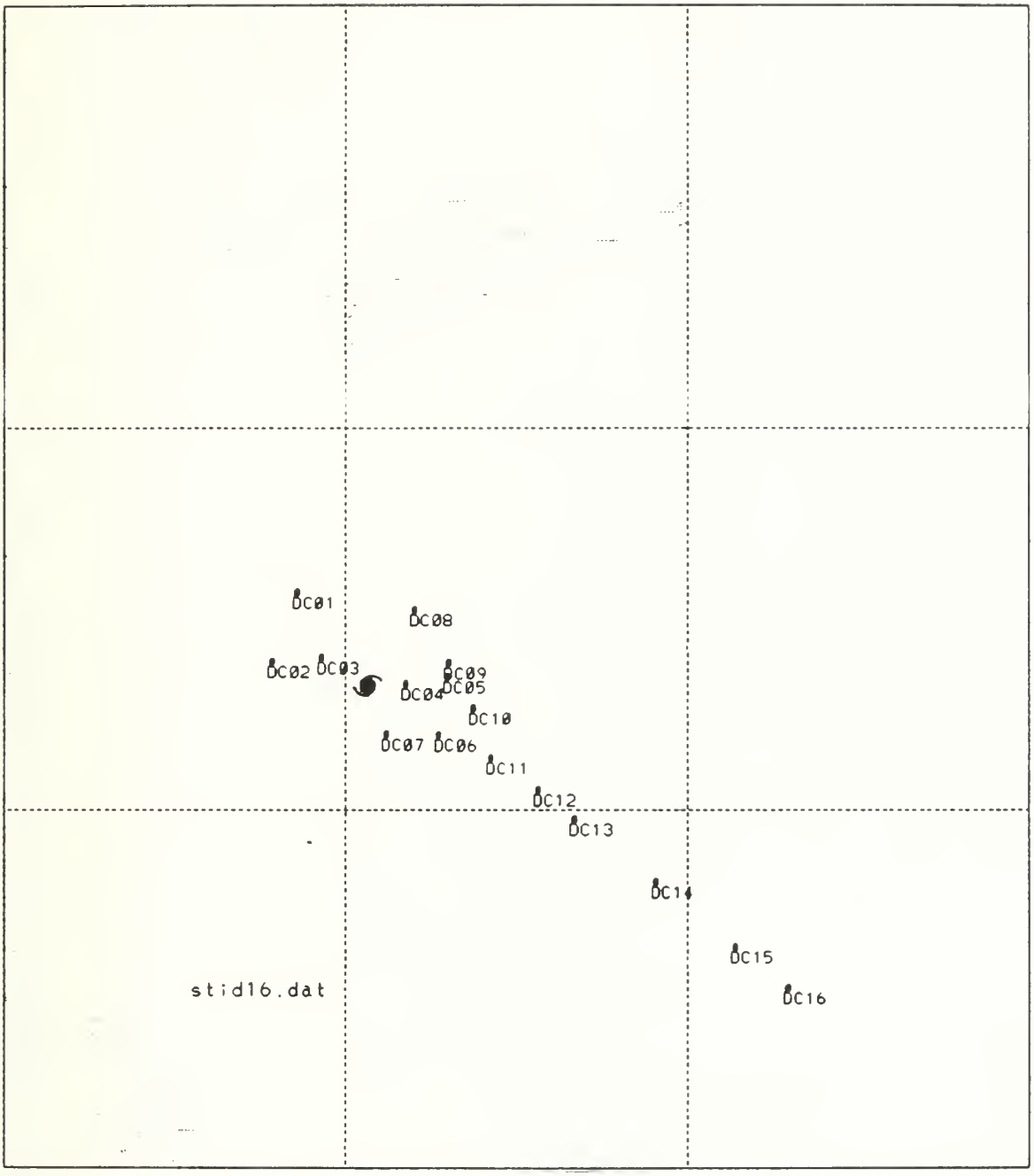

Figure 4a. Positions of dropwindsondes relative to the center of the Supertyphoon Flo on 06 UTC 16 September 1990.

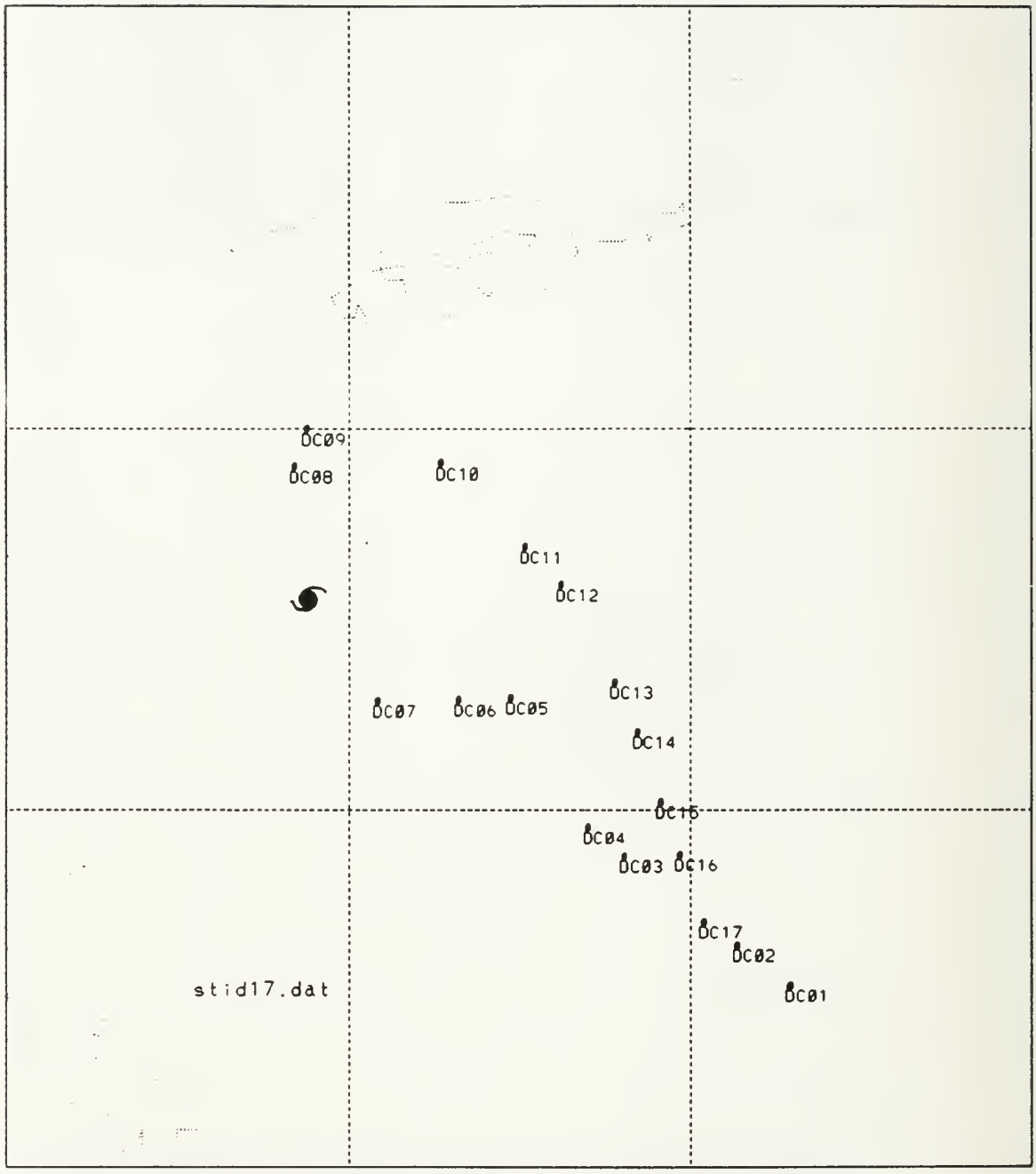

Figure 4b. As in Fig. 4a, except for 06 UTC 17 September 1990.

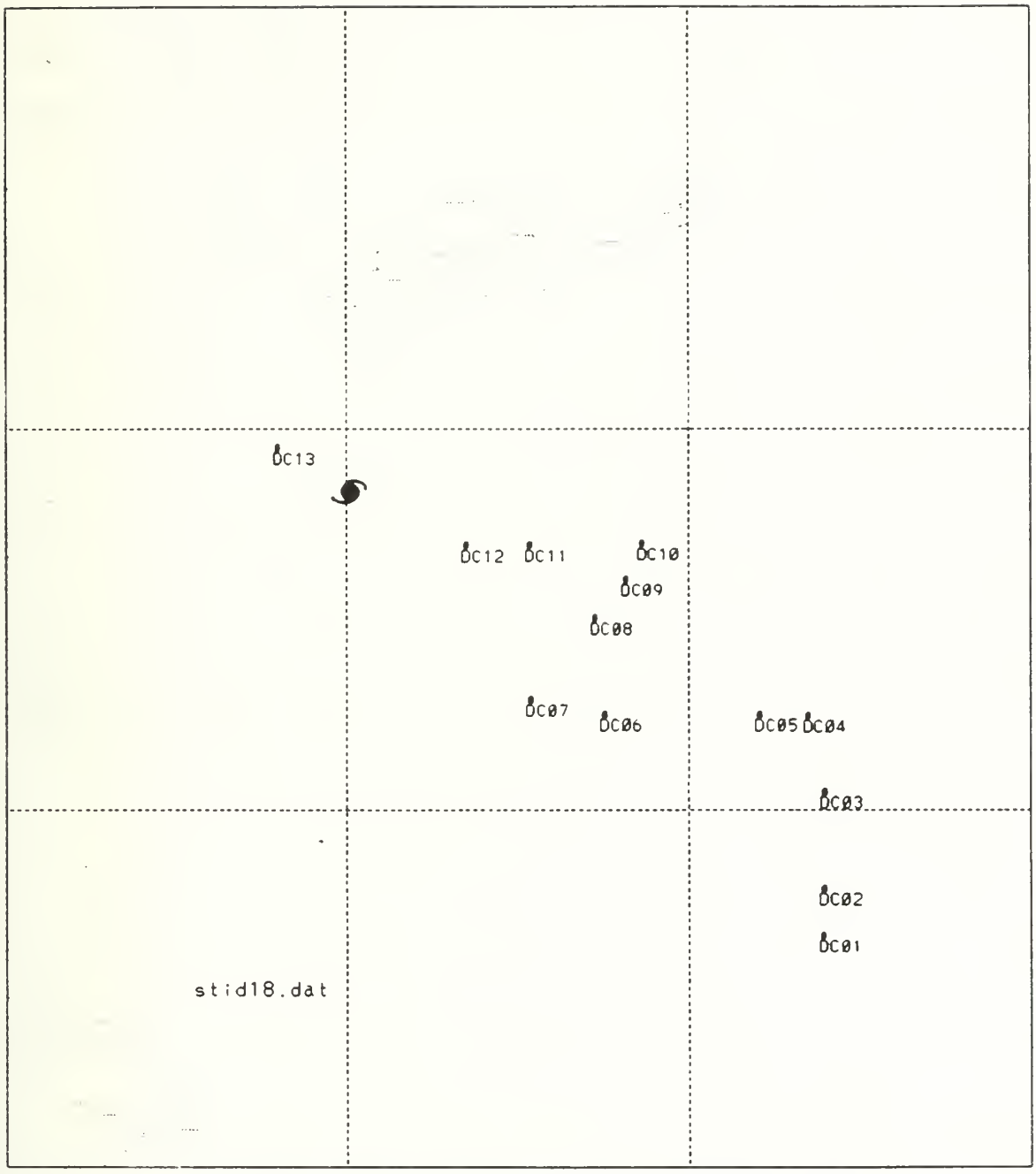

Figure 4c. As in Fig. 4a, except for 06 UTC 18 September 1990.

C. DATA PROCESSING

The convective adjustment scheme has been coded by Emanuel (1991) in a standard **FORTRAN 77** subroutine named ***CONVECT***. The following is a help file provided by Emanuel for the subroutine ***CONVECT***.

The ***CONVECT*** subroutine accepts the one-dimensional vertical input arrays of T, R, RS, P, and PH and returns the arrays FTH and FR as well as the scalar PRECIP. The definitions of the input arrays are:

T: Temperature in degrees Kelvin (K).

R: Mixing ratio (not specific humidity) in gm/gm (not gm/kg).

RS: Saturation mixing ratio in gm/gm.

P: Pressure in millibars (mb).

PH: Pressure (in mb) at the half level; i.e., halfway between the levels at which P,T,R and RS are defined. The first PH level is **BELOW** (i.e., at a higher pressure than) the first P level.

The output files are:

FTH: The tendency of POTENTIAL (not actual!) temperature in degrees/second. However, if the parameter **NOPT**, which is specified near the beginning of ***CONVECT***, is set to any value other than zero, FTH will return the tendencies of actual temperature in degrees C per second.

FR: The tendency of mixing ratio (not specific humidity) in (gm/gm)/second.

PRECIP: The rate of convective precipitation in mm/day.

One also needs to specify:

ND: The dimension of the arrays T, R, RS and P.

NDP1: The dimension of the array PH (usually NDP1=ND+1).

NL: The maximum number of model levels to be checked for moist convection. NL must be less than or equal to ND-1; e.g., one should never expect moist convection to penetrate above NL.

According to the help file for the subroutine ***CONVECT***, the arrays of R and RS must be calculated from the raw dropwindsonde data values of T, P and TD (dew-point temperature) before the model is run. In this study, the subroutine **ESAT** that is used in the Dynamical Weather Prediction Model (see Appendix A) is utilized for calculation of the water-vapor pressure e, which results from P and TD, and the saturation vapor pressure e_s, which is calculated by P and T. Then, the mixing ratio R and saturation mixing ratio RS are given by

$$R = 0.622 \frac{e}{p - e} \quad , \qquad (4\text{-}1)$$

$$RS = 0.622 \frac{e_s}{p - e_s} \quad . \qquad (4\text{-}2)$$

Some thermodynamic constants that are consistent with those in calling program (see Appendix B) also are specified, since the vertical thermodynamic structure of the atmosphere is taken as a starting point in this scheme.

V. RADIATIVE-CONVECTIVE EQUILIBRIUM SIMULATION

A. USING A PARTICULAR SOUNDING FROM THE TROPICAL WESTERN PACIFIC

A radiative-moist convective equilibrium calculation was performed by Emanuel (1991), who referred to it as a straightforward test of this new scheme. He used a constant cooling rate of 3×10^{-5} K s^{-1} (2.6°C day^{-1}) from the upper level (150 mb) to the lower troposphere (1000 mb). This cooling rate was compensated by fluxes of sensible heat and moisture from the ocean, calculated according to the bulk aerodynamic drag law:

$$Q_s = C_D |V| (\theta^s - \theta^1) \qquad (5\text{-}1)$$

$$Q_e = C_D |V| (r^{*s} - r^1) \quad , \qquad (5\text{-}2)$$

where C_D is a dimensionless exchange coefficient, here taken to be 2×10^{-3}, $|V|$ is a mean surface wind (m s^{-1}), θ^s is the potential temperature of the sea surface, and r^{*s} is the saturation mixing ratio at the sea-surface temperature and pressure; θ^1 and r^1 are the model-determined values of potential temperature and mixing ratio at the lowest grid point from the sounding. In his control simulation, Emanuel used $|V|=5$ m s^{-1} and $\theta^s=300$ K at a pressure of 1025 mb.

The model was run by Emanuel (1991) with a particular sounding from the tropical western Pacific. It was integrated in 20-minute time steps to 800 hours. The vertical grid pressure interval was 50 mb up to 200 mb, and then 25 mb up to 100 mb, for a total of 21 vertical levels.

The results of the radiative-moist convective equilibrium calculations are shown in Figs. 5a-h for the entire integration period. The time evolution of the convective precipitation (mm day^{-1}) in Fig. 5a is smoothed with a 36-hour running mean. The lowest model level potential temperature (K) and mixing ratio (g kg^{-1}) are shown in Fig. 5b and 5c, respectively. Tendencies of potential temperature (K day^{-1}) due to various processes, averaged over the last 100 hours of the model integration, are shown in Fig. 5d. The convective heating balanced the radiative cooling except in the lower boundary layer and near the tropopause. In the lower boundary layer, the surface sensible heat fluxes were important heat sources. In addition, convection is cooling the boundary layer by rain evaporation. At the upper boundary, an uncompensated cooling is produced because the **INB** was above the level of neutral buoyancy (Emanuel 1991).

Tendencies of mixing ratio (g kg^{-1} day^{-1}) are shown in Fig. 5e. Detrainment of water by convective drafts and moistening by evaporation or precipitation in the interior balanced the drying by subsidence in the environment. Near the surface, the surface evaporation balances drying by downdrafts.

The relative humidity profile is shown in Fig. 5f. Remember that the humidity at 1000 mb is not that at sea level. Emanuel pointed out that this somewhat unrealistically sharp decrease of relative humidity in the middle troposphere was related to the

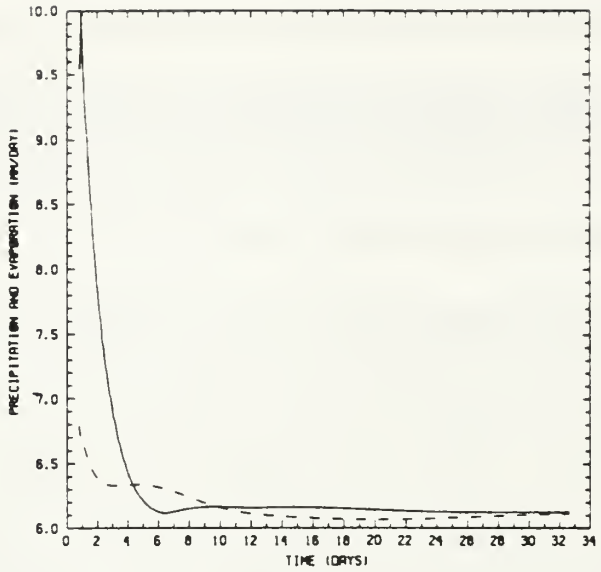

Figure 5a. Evolution with time (days) of the convective precipitation (solid) and surface evaporation (dashed) in mm/day after smoothing with a 36-h running mean (Emanuel 1991).

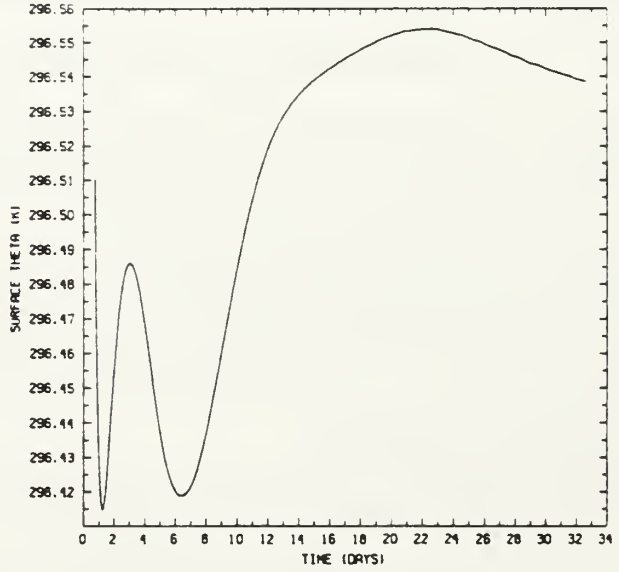

Figure 5b. Evolution with time (days) of the lowest model level potential temperature (K) after smoothing with a 36-h running mean (Emanuel 1991).

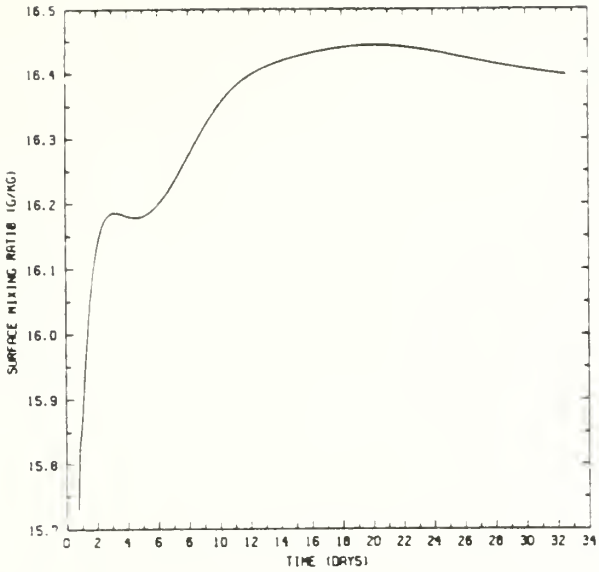

Figure 5c. Evolution with time (days) of the lowest model level mixing ratio (g/kg) after smoothing with a 36-h running mean (Emanuel 1991).

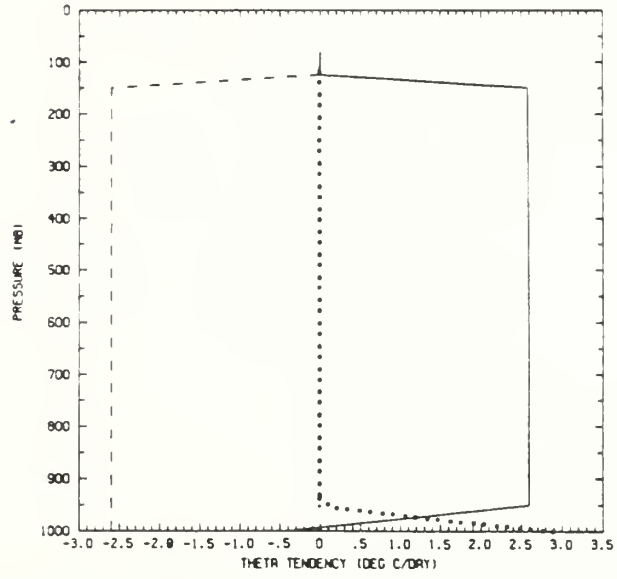

Figure 5d. Tendencies of potential temperature (K/day) averaged over the last 100 hours of model run. Solid line: convective processes. Dashed line: radiative cooling. Dotted line: surface fluxes (Emanuel 1991).

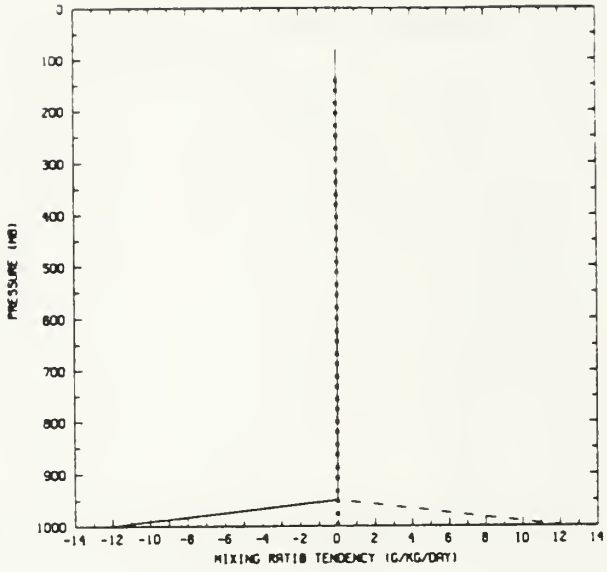

Figure 5e. Tendencies of mixing ratio (g/kg/day) averaged over the last 100 hours of model run. Solid line: convective processes. Dashed line: surface fluxes (Emanuel 1991).

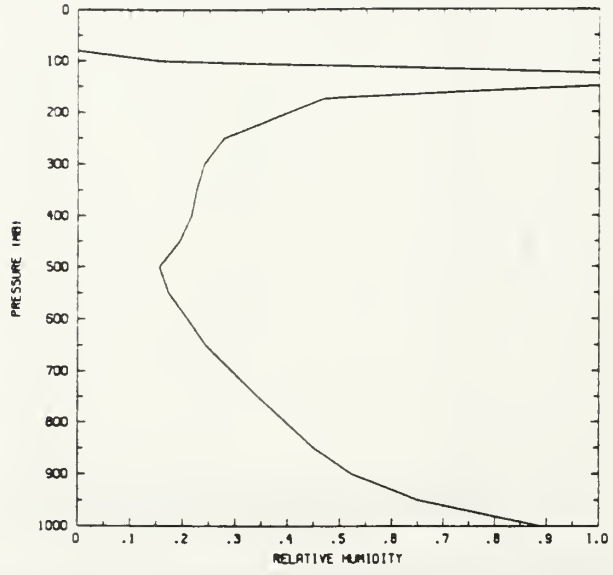

Figure 5f. Relative humidity averaged over the last 100 hours of the simulation (Emanuel 1991).

unrealistically deep layer of imposed radiative cooling in the air subsiding above the convective boundary layer. This decrease was also related to the low equivalent potential temperature (θ_e) in the lower troposphere as mentioned previously (figure not shown) which affords a large potential for downdrafts driven by the evaporation of precipitation falling from a cloud into the dry air. Fig. 5g shows the fractional areas (σ^i) covered by undilute updrafts (M^i), averaged over the last 100 hours of the integrations. These σ^i should not be interpreted as fractional areas of clouds themselves. The fractional areas (σ^i) show a sharp peak representing shallow drafts, or clouds, around 900 mb. Figure 5h shows the average buoyancy of a lifted subcloud-layer parcel. Significant amounts of buoyancy are found in the upper and lower troposphere.

As mentioned in the previous section, the vertical profiles of relative humidity were very sensitive to the model parameters. An experiment with smaller fixed value of σ ($=10^{-4}$) was performed by Emanuel (1991), as shown in Figs. 6a-b. The time evolution of precipitation rate (Fig. 6a) has been reduced and the convection has become steady, which causes changes in the equilibrium temperature and water vapor distributions as the atmosphere attempts to compensate for insufficient mass flux by increasing the amount of instability. However, the precipitation rate still reaches a nearly steady state. The buoyancy profile in Fig. 6b with the σ^i fixed at 10^{-4} has positive buoyancy all the way to the tropopause. The relative humidity with different model parameters is shown in Figs. 7a-d. For a σ value of 10^{-3} (Fig. 7a), the relative humidity in the lower troposphere is less than in the control experiment.

Emanuel performed two experiments (Figs. 7b and 7c) to demonstrate the model sensitivity to the specification of ϵ^i and σ_s^i. These experiments contrast $\epsilon^i=1$ for all i, which means all of the condensed water was converted to rain, and $\sigma_s^i=0$ except below cloud base, which means all of the rain did not fall into environment. In these two experiments, convection still moistened the upper troposphere. Using $\epsilon^i=0.5$ with $\sigma_s^i=0.15$ above cloud base (Fig. 7c), the humidity profile exhibited saturation through a deeper layer in the upper troposphere. On the other hand, it resulted in excessive detrainment of condensed water at upper levels. When the fraction of σ_s^i was increased to 0.3 (Fig. 7d), the main difference between the relative humidity in this experiment and that of the control (Fig. 5f) was a more moist lower troposphere due to evaporation. From the results above, it is important to note that water vapor still detrained from updrafts and this kept the relative humidity high in the upper troposphere.

As mentioned in the previous section, specification of σ_s^i is more difficult, since the amount of precipitation falling back through clouds, as opposed to falling through clear air, is highly dependent on the exact configuration of the cloud, its slope, presence of anvil, etc. Accordingly, this new version modified by Emanuel set $\sigma_s^i=0.15$. Also, the fraction areas, σ^i, were calculated in a completely different way. They were adjusted downward whenever the minimum buoyancy below level i was less than a critical and positive value of DTCRIT = 0.2, and upward when the minimum buoyancy exceeded this value. Here, the DTCRIT is the critical buoyancy (K) used to adjust the approach to quasi-equilibrium.

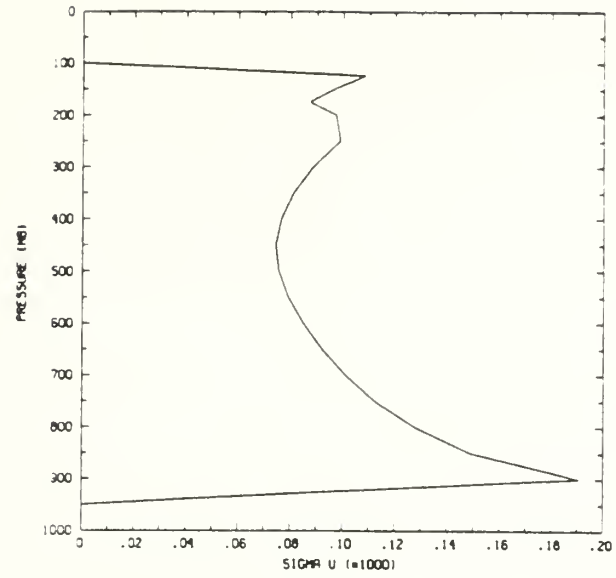

Figure 5g. Fractional areas, σ^i, (10^{-3}) covered by undilute updrafts carrying mass flux M^i averaged over the last 100 hours of model run (Emanuel 1991).

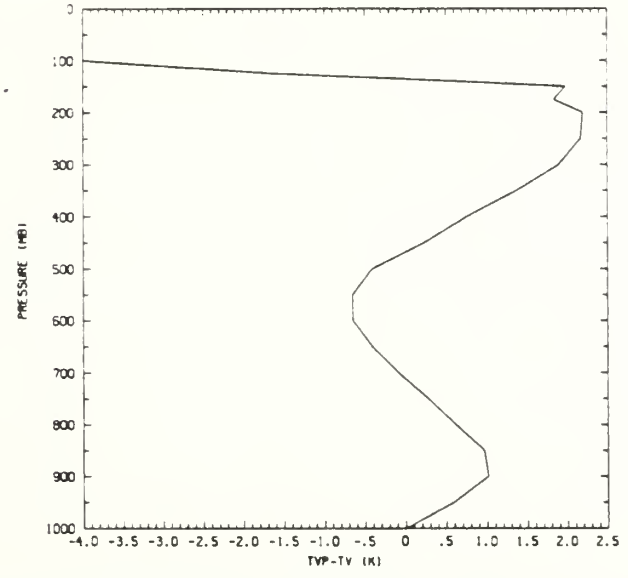

Figure 5h. Buoyancy (K) averaged over the last 100 hours of the simulation (Emanuel 1991).

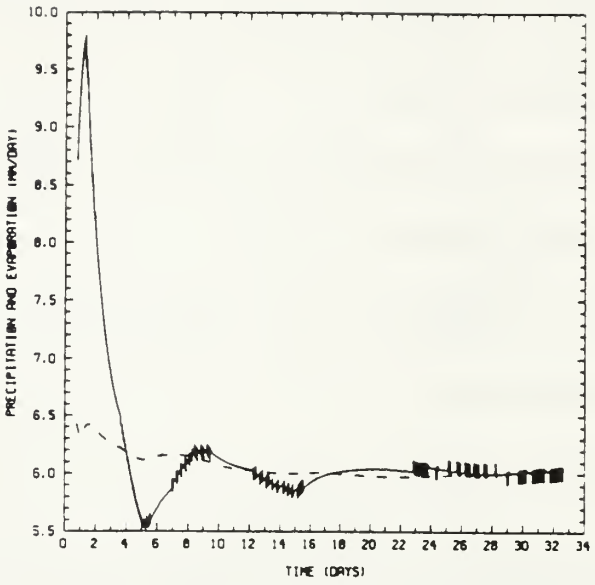

Figure 6a. Evolution with time (days) of the convective precipitation (solid) and surface evaporation (dashed) but for smaller σ^i ($=10^{-4}$), in mm/day after smoothing with a 36-h running mean (Emanuel 1991).

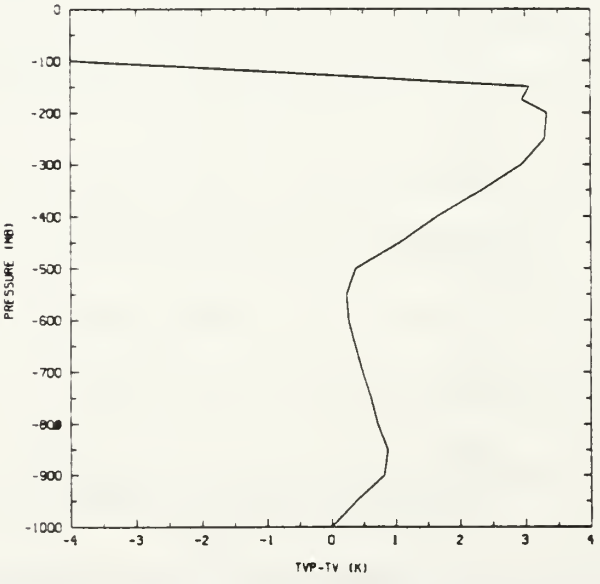

Figure 6b. Buoyancy averaged over the last 100 hours model run, except for smaller σ^i ($=10^{-4}$) value (Emanuel 1991).

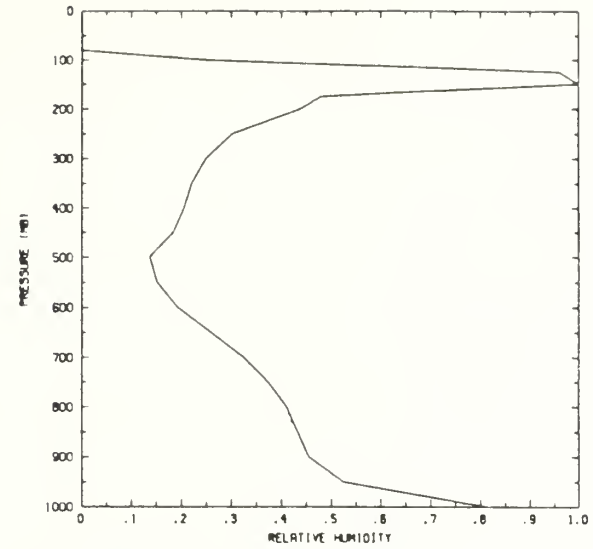

Figure 7a. Relative humidity averaged over the last 100 hours of model run, except for $\sigma=10^{-3}$ value (Emanuel 1991).

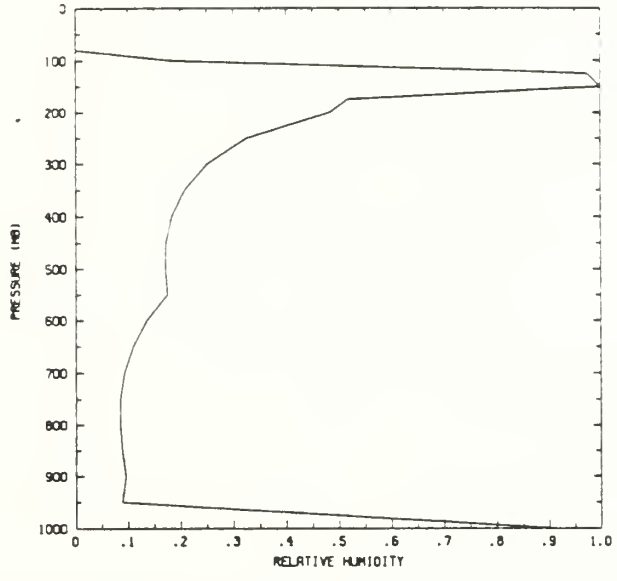

Figure 7b. Relative humidity averaged over the last 100 hours of an equilibrium experiment in which $\epsilon^i=1$ throughout, with $\sigma_s^i=0$ except below cloud base (Emanuel 1991).

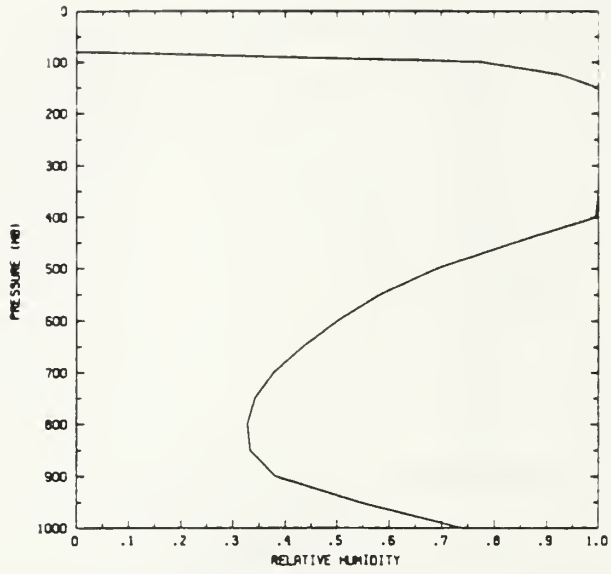

Figure 7c. Relative humidity averaged over the last 100 hours of an equilibrium experiment in which $\epsilon^i=0.5$ everywhere with $\sigma_s^i=0.15$ above cloud base (Emanuel 1991).

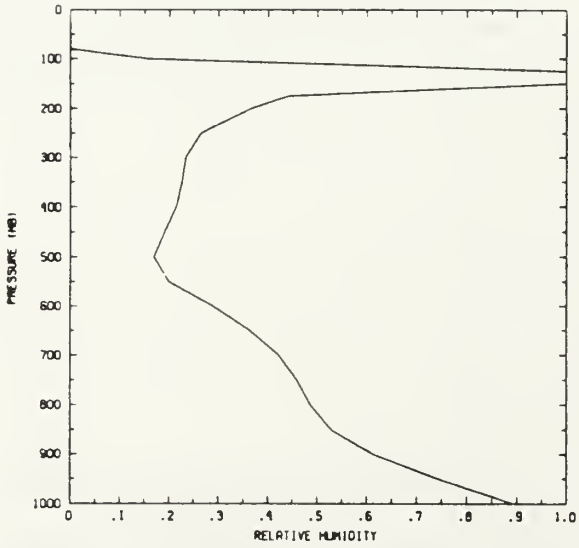

Figure 7d. Relative humidity averaged over the last 100 hours of an equilibrium experiment in which $\epsilon^i=0.5$ everywhere with $\sigma_s^i=0.3$ above cloud base (Emanuel 1991).

B. USING TCM-90 DROPWINDSONDE DATA

For convenience, the sea surface temperature was taken to be 29°C (Fig. 8) for all inputs. Most of the dropwindsondes provided the measured wind speed above 1000 mb. For those soundings with the measurement of wind speed available between 900 mb and 1000 mb, the wind speeds at the top of the boundary layer were estimated from the measurement and reduced to about 80 % to represent the approximate surface wind speed. As to the soundings without wind speed measurement, we simply used the nearest available sounding data (for convenience) as input to run the model. Since the surface fluxes of heat and moisture are dependent on the wind speed, the wind speed plays an important role in the time integration. The wind speeds for all dropwindsonde locations and the relative distances between dropwindsonde stations and the center of **Supertyphoon Flo** are listed in Table III.

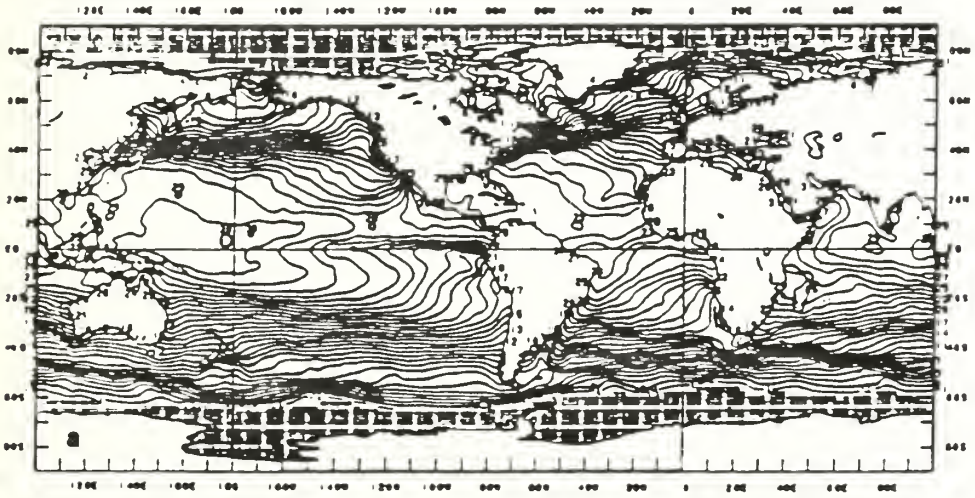

Figure 8. Monthly mean sea surface temperature with contour interval = 1°C for September 1990 (adapted from Climate Diagnostics Bulletin of U.S. Department of Commerce).

TABLE III. RELATIVE DISTANCE (° LAT.) BETWEEN DROPWINDSONDE STATION AND THE CENTER OF SUPERTYPHOON FLO AND ESTIMATED SURFACE WIND SPEED OF EACH SOUNDING.

TIME	06 UTC 16 Sept.		06 UTC 17 Sept.		06 UTC 18 Sept.	
STID	Dist.(°)	Vel.(m/s)	Dist.(°)	Vel.(m/s)	Dist.(°)	Vel.(m/s)
DC01	3.24	12.76	17.51	6.38	18.17	5.58
DC02	2.89	17.55	15.61	15.95	17.36	3.99
DC03	1.56	22.33	11.52	5.58	15.91	1.60
DC04	1.12	26.32	10.19	4.79	14.54	0.80
DC05	2.43	20.74	6.40	30.70	13.24	1.60
DC06	2.45	21.53	5.08	12.76	9.39	7.14
DC07	1.40	25.15	3.32	22.33	7.53	7.98
DC08	2.43	23.14	3.46	13.56	7.79	8.77
DC09	2.43	22.33	4.37	9.57	8.29	8.77
DC10	3.13	22.33	5.18	11.96	8.56	8.77
DC11	4.07	15.15	6.42	14.36	5.33	16.75
DC12	5.70	12.76	7.35	14.36	3.58	19.14
DC13	7.31	8.77	9.20	7.98	2.46	21.53
DC14	9.92	3.99	10.22	2.39		
DC15	12.87	4.79	11.61	4.79		
DC16	14.78	13.37	12.81	3.99		
DC17			14.44	4.78		

In this study, the convection model was run with a 20-minute time step to predict the 24-hour mean precipitation rates. The environmental forcings in the tendency of temperature, $\partial T/\partial t$, and the tendency of moistening, $\partial R/\partial t$ were specified according to:

if $P_{950} \leq P \leq P_0$

$$\frac{\partial T}{\partial t} = -\gamma + FTH + \frac{P - P_{950}}{P_0 - P_{950}} \times \frac{Q_s}{500} \qquad (5\text{-}3a)$$

$$\frac{\partial R}{\partial t} = FR + \frac{P - P_{950}}{P_0 - P_{950}} \times \frac{Q_R}{500} \qquad (5\text{-}3b)$$

if $P < P_{950}$

$$\frac{\partial T}{\partial t} = -\gamma + FTH \qquad (5\text{-}3c)$$

$$\frac{\partial R}{\partial t} = FR \qquad (5\text{-}3d)$$

where γ ($=3\times10^{-5}$ K s^{-1}) is a constant radiative cooling, FTH is the convective heating calculated from the model, and FR is the convective moistening. Q_S and Q_R are surface heat and moisture fluxes. P_0 is 1000 mb, P_{950} is 950 mb, and 500 m is the approximate layer depth between P_0 and P_{950}. The net tendency of heating $\partial T/\partial t$, in the layer below P_{950} was the sum of radiative cooling, convective heating and surface flux, and in the layer above 950 mb was due only to radiative cooling and convective heating. Similarly, the net tendency of moistening $\partial R/\partial t$, in the layer below P_{950} was the sum of convective

moistening and surface flux, and in the layer above 950 mb was due only to the convective moistening. In this calculation, the parameter ϵ^i is the same as equation (3-11), σ_d=0.01 and σ_s^i=0.15 are similar to that of Emanuel (1991), except that the σ^i are adjusted according to the critical buoyancy 0.2 K, which is used to adjust the approach to the quasi-equilibrium (discussed in previous section).

The 24-hour mean precipitation rates predicted from the dropwindsondes are listed in Table IV. We will discuss these rates in the next section.

TABLE IV. PREDICTED AVERAGE 24 HOUR PRECIPITATION (MM/DAY) BASED ON THE DROPWINDSONDES IN SUPERTYPHOON FLO ON 16, 17 AND 18 SEPTEMBER 1990.

Dropwindsonde stations	Precipitation of 16 September	Precipitation of 17 September	Precipitation of 18 September
DC04	6.99	0.57	0.27
DC02	13.63	3.15	0.00
DC03	12.22	0.53	0.00
DC04	15.69	0.49	0.00
DC05	2.46	12.21	0.00
DC06	15.86	2.59	0.83
DC07	12.30	15.18	4.43
DC08	2.33	1.85	13.02
DC09	14.42	1.27	4.78
DC10	13.16	1.64	0.00
DC11	2.58	1.20	1.18
DC12	4.41	4.32	4.78
DC13	3.79	0.32	9.25
DC14	1.92	0.01	
DC15	1.93	0.42	
DC16	5.45	0.35	
DC17		0.09	

C. HORIZONTAL DISTRIBUTION OF PRECIPITATION PREDICTED BY THE MODEL

Rainfall associated with tropical cyclones is both beneficial and harmful. Although the rains contribute to the water needs of the areas traversed by the cyclone, the rains are harmful when the amount is so large as to cause flooding.

Using a water budget and composite data to calculate the average precipitation, Gray (1981) found that average precipitation rates over 80 mm day^{-1} could be expected within 2° latitude of a Pacific typhoon. In the ring 2°-4° latitude from the center, the average rate falls off to about 25 mm day^{-1} and to less than 10 mm day^{-1} outward of 4°. Gray also makes two important points for composite averages: (i) precipitation near the center is more closely associated with average outer wind strength than with central core intensity; and (ii) rainfall accumulation at a specific site is strongly associated with forward speed and tends to be heaviest for tropical cyclones that stall.

The precipitation rate for each dropwindsonde on 16 September and the corresponding satellite picture are shown in Figs. 9 and 10, respectively. The precipitation rates for DC03 (12.22 mm/day), DC04 (15.69 mm/day) and DC07 (12.30 mm/day) on 16 September (Tables III and IV) are very small in comparison with Gray's calculation within 2° latitude. In the ring 2°-4° latitude, the rainfall rates are also small and soundings DC05 (2.46 mm/day) and DC08 (2.33 mm/day) even have a rate less than 3 mm/day. Outward of 4° latitude, the precipitation rates are all less than 10 mm/day as in Gray's calculation.

The precipitation rates and satellite picture for 17 September are shown in Figs. 11 and 12. For DC07 (15.18 mm/day) and DC08 (1.85 mm/day) in the ring 2°-4° latitude (Table III), the precipitation rates are very small, especially for DC08 has rate even less than 2 mm/day (Fig. 12). Another sounding (DC05) has a precipitation rate larger than 12 mm/day because of the strong surface wind speed (30.70 m/s). The precipitation rates outward of 4° latitude have values smaller than 5 mm/day as one would expect (Fig. 12).

The estimated precipitation rates and satellite picture on 18 September are shown in Figs. 13 and 14 respectively. The largest value of rainfall is 13.02 mm/day (DC08) and is located on a nearby cloud band. Two stations within 2°-4° latitude, DC12 (4.78 mm/day) and DC13 (9.25 mm/day), again have small precipitation rates (Tables III and IV). In regions outward of 4° latitude, all estimates that have small precipitation rates or zero precipitation are in cloud-free areas. Although the values of precipitation are small in comparison with Gray's calculation, the precipitation estimates located on major cloud bands have larger rates than the sparsely cloud-covered areas, where one would not expect to have strong convection and rainfall.

Recently, LCDR George M. Dunnavan of Naval Postgraduate School has done a comparison of the dropwindsondes and adjacent rawinsondes and concluded the moisture values of the dropwindsondes are significantly low. This could be one reason for the predicted small precipitation rates. According to the results shown in this section, we performed some simulations to examine other possible explanations for the low precipitation rates calculated with the Emanuel model.

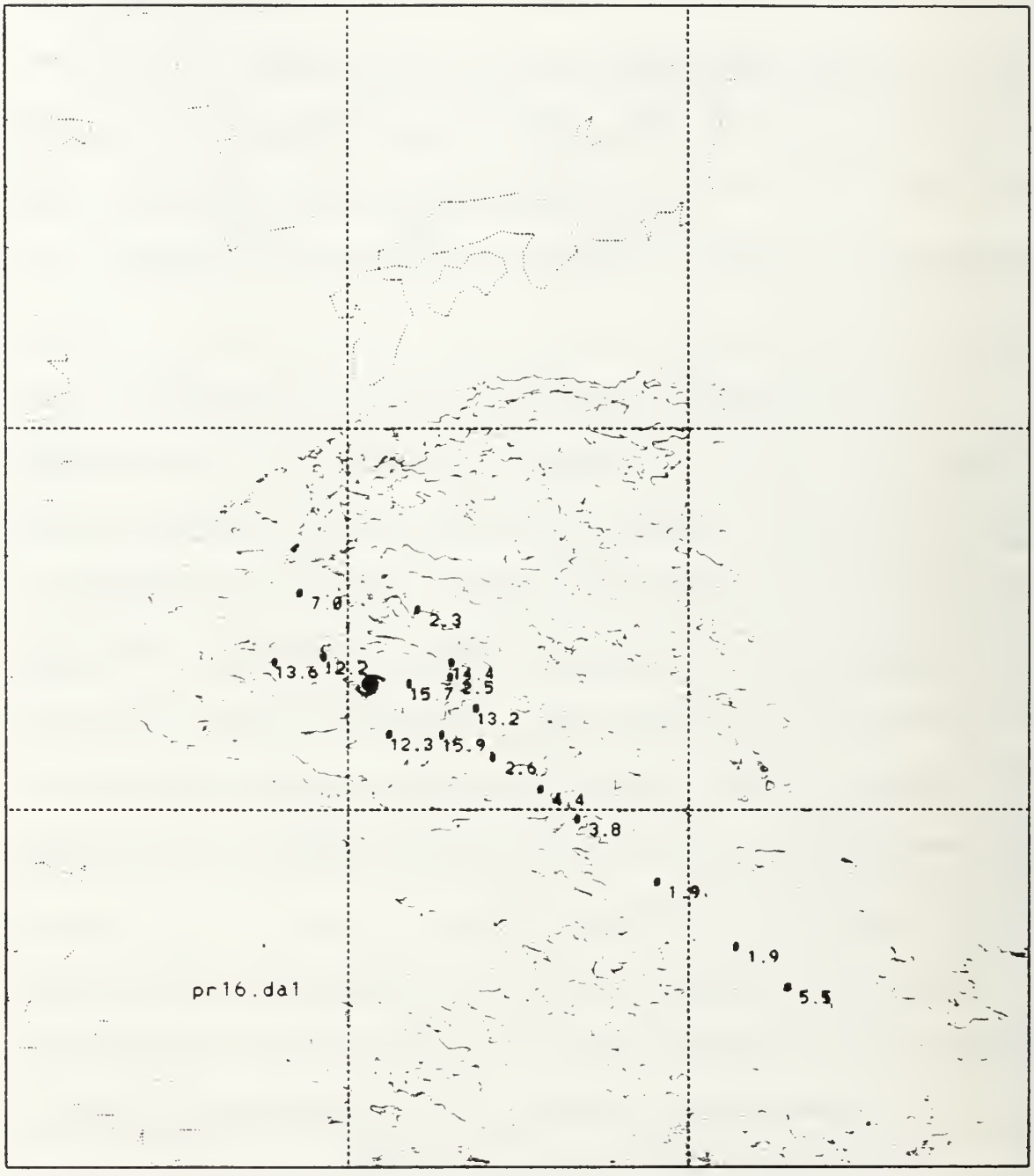

Figure 9. Predicted precipitation rate (mm/day) for the soundings of 16 September 1990.

Figure 10. IR satellite imagery of the Supertyphoon Flo on 16 September 1990.

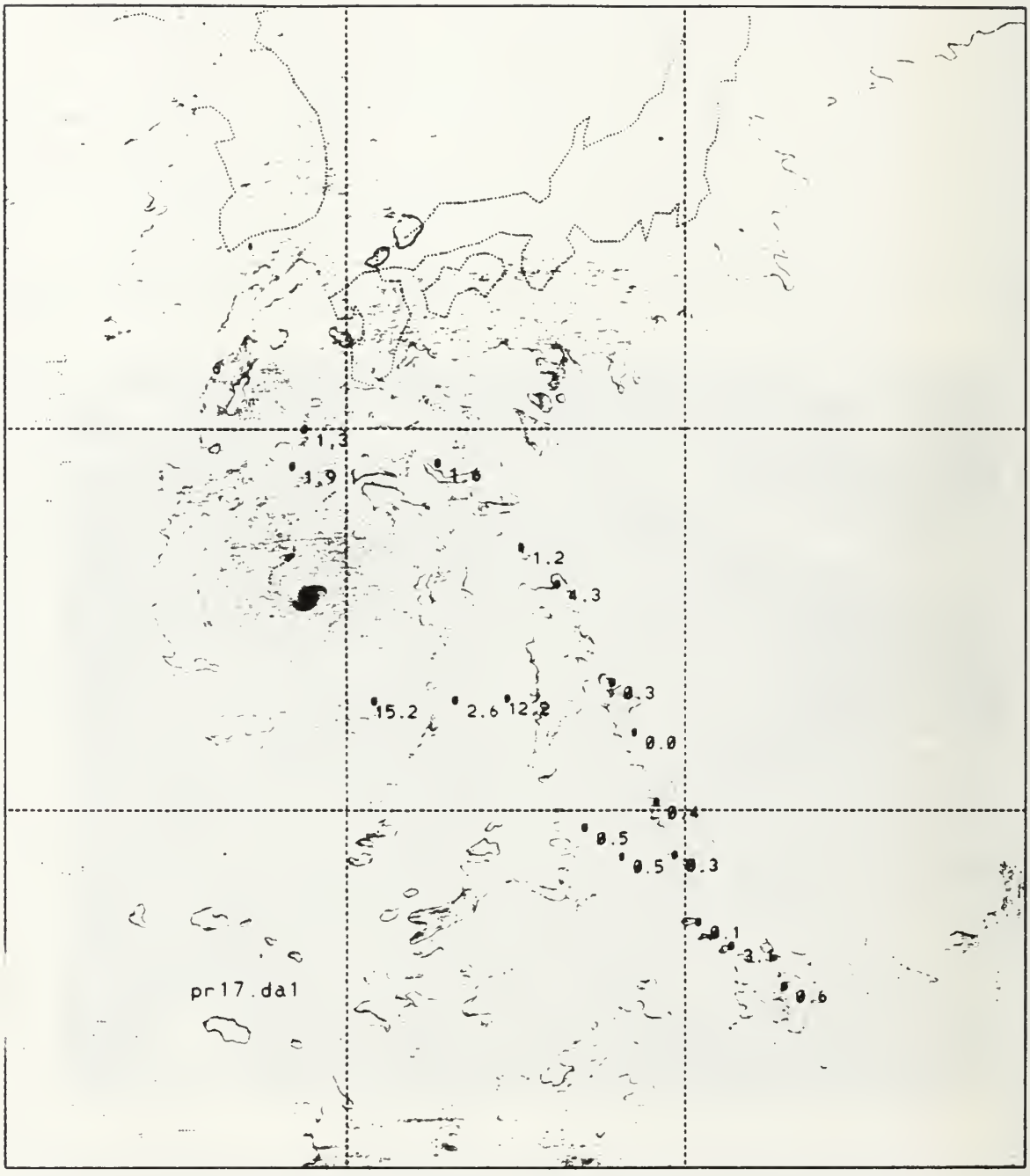

Figure 11. Predicted precipitation rate (mm/day) for the soundings of 17 September 1990.

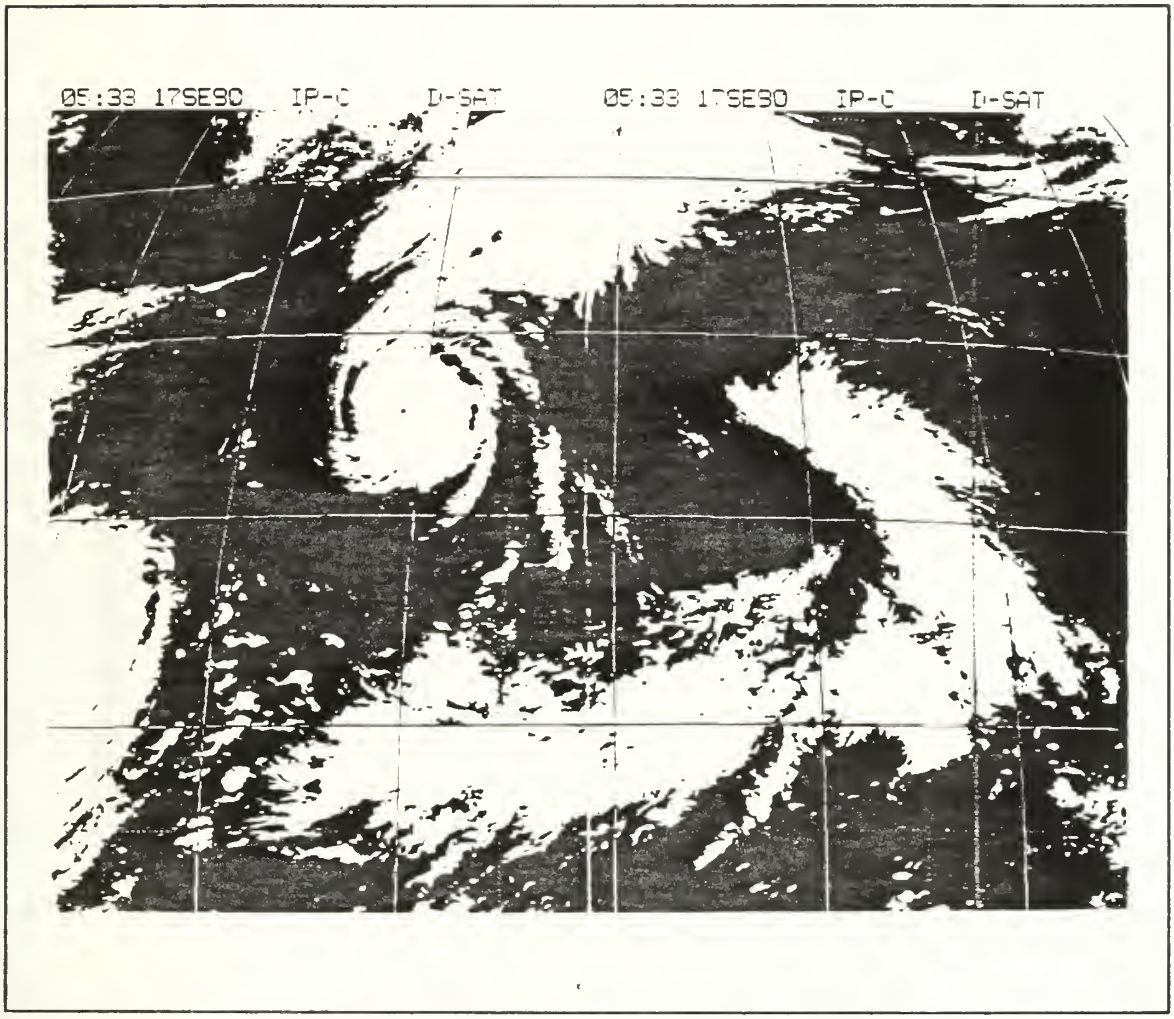

Figure 12. IR satellite imagery of the Supertyphoon Flo on 17 September 1990.

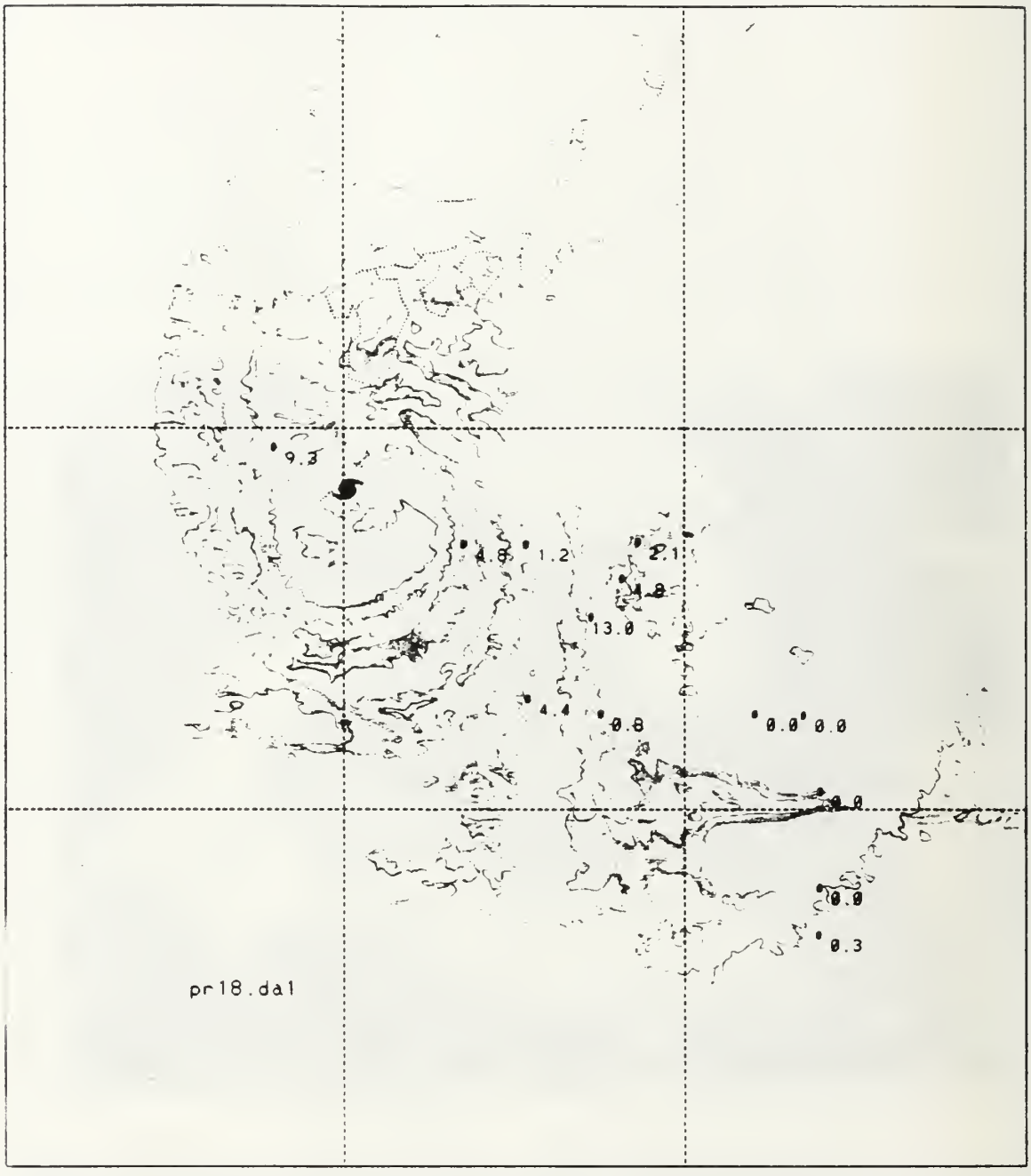

Figure 13. Predicted precipitation rate (mm/day) for the soundings of 18 September 1990.

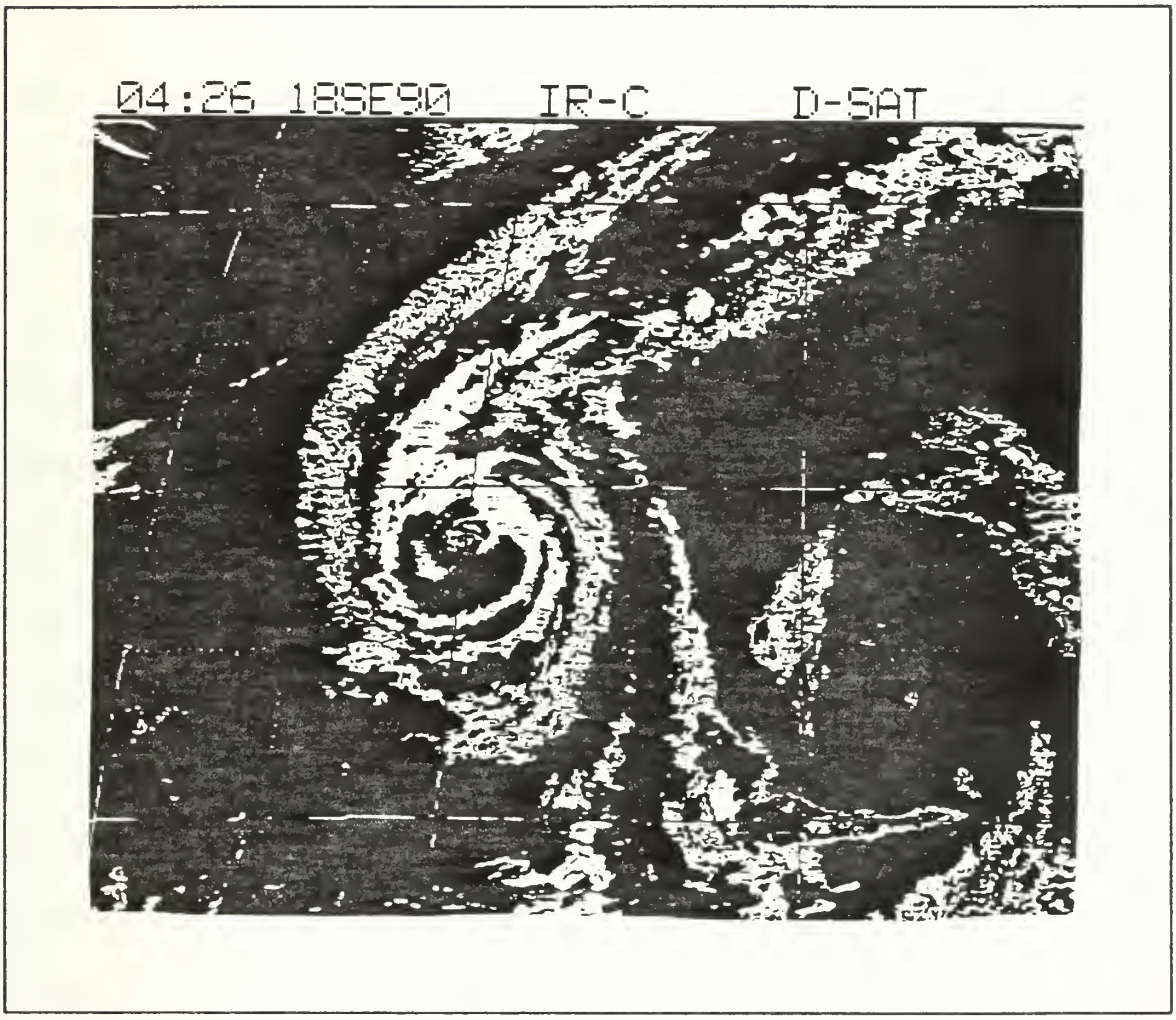

Figure 14. IR satellite imagery of the Supertyphoon Flo on 18 September 1990.

D. SENSITIVITY SIMULATIONS

Several simulations were designed to examine the sensitivity of the model results to the inputs of surface wind speed and radiative cooling rates, and to the specification of precipitation efficiency. Furthermore, 13 nearby rawindsondes were chosen and used to compare with the precipitation rates of dropwindsondes.

1. Case A

In this case, the model was re-run with changes in the imposed surface velocity of $\pm$ 2.5, $\pm$ 5.0 and $\pm$ 7.5 m/s respectively. These variations are relative to the estimated surface winds of V_4=26.32 m/s (for DC04), V_5=20.74 m/s (for DC05), V_6=21.53 m/s (for DC06) and V_9=22.33 m/s (for DC09), which are the wind speeds for the control case. The precipitation rates with those speeds were 15.69, 2.46, 15.86 and 14.42 mm/day respectively. The precipitation rates increased with increasing velocity as expected (Table V). For all except the third soundings, the range of precipitation rates for a 15 m/s difference in surface speed is 2-5 mm/day. However, sounding DC06 is much less sensitive to surface wind speed as the range of precipitation is only about 1 mm/day. These increased precipitation rates are due to the increase in surface moisture fluxes, which provides the atmospheric column with a larger moisture

In conclusion, the model is sensitive to the imposed surface wind speed, but this does not explain the generally low precipitation rates near the center.

TABLE V. PREDICTED PRECIPITATION RATES (MM/DAY) OF FOUR SOUNDINGS TO TEST SENSITIVITY TO THE IMPOSED SURFACE WIND V_i (CONTROL VELOCITIES ARE V_4=26.32, V_5=20.74, V_6=21.53, V_9=22.33 M/S).

STID	V_i-7.5	V_i-5.0	V_i-2.5	V_i+2.5	V_i+5.0	V_i+7.5
DC04	14.46	15.00	15.42	16.08	16.17	16.80
DC05	0.93	1.50	2.06	3.21	3.35	4.86
DC06	15.01	15.18	15.49	16.08	16.27	16.30
DC09	10.28	12.37	13.61	15.33	15.49	15.32

2. Case B

In this case, the radiative cooling γ was changed from 0 to 3.0×10^{-5} K/s with an increment of 0.5 for each sounding. The effect of decreasing the radiative cooling to the precipitation rates is listed in Table VI. The precipitation rates are decreased when the radiative cooling rates are decreased from the control value of 3.0×10^{-5} K/s. The range of precipitation rates for sounding DC05 is only 1.78 mm/day, and this rate is not continually decreased as in the other cases. For the other three soundings, the range of precipitation rates for a 3.0×10^{-5} K/s decrease in the radiative cooling is 3-7 mm/day, which is a larger range of precipitation rates than in Table V. If the atmosphere is radiatively cooled at a lower rate, then the model predicts the precipitation rate would be smaller.

Unfortunately, this test does not assist in explaining the too-low precipitation rates near the center. With a thick cloud overcast near the center, the net radiative

cooling to space should be smaller. Here, we see that a reduction from larger radiative cooling rates (expected in clear dry outer region of typhoon) does not increase precipitation.

TABLE VI. PREDICTED PRECIPITATION RATES (MM/DAY) OF FOUR SOUNDINGS TO TEST SENSITIVITY TO THE EFFECT OF DIFFERENT RADIATIVE COOLING RATES (10^{-5} K/S).

STID	γ=0.0	γ=0.5	γ=1.0	γ=1.5	γ=2.0	γ=2.5	γ=3.0
DC04	12.24	12.85	13.39	14.10	14.94	15.07	15.69
DC05	0.68	0.68	0.37	2.11	1.54	2.49	2.46
DC06	12.85	13.46	13.98	14.42	14.93	15.27	15.86
DC09	7.77	9.02	9.34	11.68	13.39	13.64	14.42

3. Case C

In this case, we set the precipitation efficiencies ϵ^i=0.5 everywhere (versus cases A and B) and re-ran the model with the changes of imposing velocities as in case A to further estimate the changes of the precipitation rates for those four soundings. Here, ϵ^i=0.5 everywhere seemed appropriate for the inner region of typhoon where humidities should be nearly saturated and evaporation should be large. Decreased precipitation rates, as expected, are found with decreasing ϵ^i (Table VII). The range of precipitation rates for the first three soundings with a 15 m/s difference in surface wind speed is less than 2 mm/day. Although sounding DC09 is still more sensitive to these changes, the range of precipitation rates has been reduced to 2.66 mm/day, which is

about 1/2 of case A. However, sounding DC06 has a range of 1.93 mm/day, which is larger than that in case A (1.29 mm/day).

TABLE VII. PREDICTED PRECIPITATION RATES (MM/DAY) OF FOUR SOUNDINGS TO TEST SENSITIVITY TO THE PRECIPITATION EFFICIENCIES ϵ^i=0.5 EVERYWHERE AND THE IMPOSED SURFACE WIND V_i (CONTROL VELOCITIES ARE V_4=26.32, V_5=20.74, V_5=21.53, V_9=22.33 M/S).

STID	V_i-7.5	V_i-5.0	V_i-2.5	V_i+2.5	V_i+5.0	V_i+7.5
DC04	6.50	6.88	7.18	7.75	8.04	8.24
DC05	0.48	1.03	1.01	1.87	2.05	2.25
DC06	4.84	5.21	5.56	6.22	6.53	6.77
DC09	3.41	3.73	4.32	5.40	5.81	6.07

4. Case D

In this case, we set the precipitation efficiencies ϵ^i=0.5 everywhere as in case C and re-run with decreasing the radiative cooling rate from 3 to 0 in an increment of 0.5×10^{-5} K/s to see the changes of the precipitation rates. The range of precipitation rates has been further reduced for each sounding (Table VIII) as expected in comparison with case B (Table VI). Sounding DC05 now has a consistent decrease in precipitation with decreasing radiative cooling, but the range is only 0.66 mm/day. This test does not give a good reason to explain the too-low precipitation rates within the ring of 4° latitude from the center of a typhoon. The effect of the imposed radiative cooling rate needs to be further investigated since it depends on whether a cloud is present.

TABLE VIII. PREDICTED PRECIPITATION RATES (MM/DAY) OF FOUR SOUNDINGS TO TEST SENSITIVITY OF PRECIPITATION EFFICIENCIES ϵ^i=0.5 EVERYWHERE AND TO THE EFFECT OF DIFFERENT RADIATIVE COOLING RATES (10^{-5} K/S).

STID	γ=0.0	γ=0.5	γ=1.0	γ=1.5	γ=2.0	γ=2.5	γ=3.0
DC04	5.42	5.84	6.21	6.54	6.84	7.16	7.49
DC05	0.41	0.47	0.54	1.17	1.24	1.33	1.07
DC06	3.95	4.28	4.57	4.92	5.30	5.62	5.85
DC09	2.50	2.73	2.83	3.65	3.79	4.33	4.66

5. Case E

We also conducted a simulation with nearby rawindsonde data collected during the **TCM-90** field experiment as inputs to compare with the dropwindsonde results. In this case, data processing procedures were the same as before and the rawindsonde data set provides a surface wind speed measurement. The predicted precipitation rates by using rawindsondes on 16 September are listed in Table IX. No ship rawindsonde data are shown here because those rawindsondes had large missing data and gaps in the vertical and thus were omitted. Fortunately, we had one rawindsonde at station 91232 with V=7.76 m/s close to the dropwindsondes DC15 (V=5.63 m/s) and DC16 (V=5.25 m/s) on 16 September. The precipitation rate for STNM 91232 is 4.93 mm/day, which is 3 mm/day larger than DC15 (1.93 mm/day) and has a comparable rate with DC16 (5.45 mm/day). STNM 47185 (10.57 mm/day) and 47138 (12.14 mm/day) were located

on a long heavy cloud-covered band and STNM 94826 (4.98 mm/day) was located in another cyclone affecting the region (Fig.10).

TABLE IX. RAWINDSONDE STATION, LATITUDE, LONGITUDE, RELATIVE DISTANCE (° LAT.), VELOCITY (M/S) AND PRECIPITATION RATE (MM/DAY) FOR 16 SEPTEMBER.

STNM	LAT.	LONG.	DIST.	VEL.	PRECIP.
94826	14.80	120.30	13.43	5.82	4.98
91232	15.07	145.43	16.87	7.76	4.93
47185	33.30	126.20	10.97	9.70	10.57
47138	36.00	129.40	12.77	7.76	12.14

There were five rawindsondes to compare with dropwindsondes on 17 September. The results are listed in Table X. In comparing the precipitation rates in Table X, STNM 91232 with small surface wind speed (V=3.88 m/s) had a much larger precipitation rate (10.75 mm/day) than dropwindsondes of DC01 (0.57 mm/day) and DC02 (3.15 mm/day), because STNM 91232 was located on long narrow cloud band. The other four stations (00002, 47918, 47971 and 47909) in Table X showed no precipitation because they were located in cloud-free areas. The precipitation rate for dropwindsonde DC14 also had zero precipitation and it was located in a cloud-free area.

TABLE X. RAWINDSONDE STATION, LATITUDE, LONGITUDE, RELATIVE DISTANCE (° LAT.), VELOCITY (M/S) AND PRECIPITATION RATE (MM/DAY) FOR 17 SEPTEMBER.

STNM	LAT.	LONG.	DIST.	VEL.	PRECIP.
91232	15.07	145.43	19.60	3.88	10.75
00002	20.00	126.00	6.31	15.52	0.0
47918	24.30	124.20	4.88	23.28	0.0
47971	27.10	142.20	13.58	13.58	0.0
47909	28.40	129.60	2.89	19.40	0.0

On 18 September, four soundings were run with the model (Table XI). STNM 47909, which was almost in the center of **Supertyphoon Flo,** had a predicted precipitation rate of only 11.98 mm/day. STNM 47827, which was within 4° latitude, had a precipitation rate of 12.81 mm/day. Both of these precipitation rates are also small in comparison with Gray's calculation, as was the case for the simulations with the dropwindsondes.

TABLE XI. RAWINDSONDE STATION, LATITUDE, LONGITUDE, RELATIVE DISTANCE (° LAT.), VELOCITY (M/S) AND PRECIPITATION RATE (MM/DAY) FOR 18 SEPTEMBER.

STNM	LAT.	LONG.	DIST.	VEL.	PRECIP.
00004	16.90	139.00	14.48	11.64	0.52
47909	28.40	129.60	0.6	30.00	11.98
47827	31.60	130.60	3.22	9.60	12.81
47807	33.60	130.40	5.20	11.64	1.33

Unfortunately, I did not have the precipitation rates measured on the DC-8 aircraft with the prototype Tropical Rainfall Measurement Mission (TRMM) radar to further support my comparison. The parameter $\epsilon^i=0.5$ everywhere seems appropriate for inner region of typhoon. In these cases, the simulations produced even smaller rates of precipitation except for DC05 dropwindsonde on 16 September, which had increased rates from 0.37 to 0.54 mm/day even with low constant radiative cooling rate $\gamma=1.0\times10^{-5}$ K/s (Tables VI and VIII). The model is sensitive to the surface wind speed, radiative cooling rate and the specification of precipitation efficiency. This modified version using rawindsondes also predicted very small precipitation rates within 4° latitude of the center of a typhoon. Therefore, we conclude that this new modified convective scheme does not predict precipitation rates well near the center of **Supertyphoon Flo** on 16, 17 and 18 September 1990.

VI. CONCLUSIONS

A cumulus convection model developed by Emanuel (1991) appears to be based as much as possible on the dynamics and microphysics of convection as found by recent detailed aircraft observations. These observations suggest that the convective process based on reversible ascent of subcloud-scale updrafts and downdrafts, mixing, and buoyancy sorting is essential in representing convection. For a variety of cases, the model produces reasonable profiles of buoyancy and relative humidity (Emanuel 1991).

Emanuel forced the model with the surface forcing and constant radiative cooling to demonstrate the sensitivity to the empirical constant that specifies how much condensed water ultimately falls out as precipitation, which controls the net heating and the vertical distribution of moistening. Both of these distributions depend on the details of cloud dynamical process and microphysical parameters (ϵ^i, σ_s^i). Consequently, the vertical profiles of relative humidity were sensitive to these parameters.

The model simulation using **TCM-90** dropwindsondes and rawindsondes show that the precipitation rates are too small within 4° latitude from cyclone center. Some larger values appeared in outer cloud bands. This new modified convective scheme was also shown to be sensitive to the specified parameter ϵ and the surface wind speed and radiative cooling values specified. Although this model produced reasonable precipitation

rates outward 4° latitude from typhoon center, it does not predict the precipitation rates well near the center of the typhoon.

As pointed out by Emanuel (1991), the main parameters of the present scheme are the parcel precipitation efficiencies (ϵ^i), which govern how much condensed water in a given parcel is converted to precipitation, and the parameter σ_s^i, which determines how much precipitation falls back through cloudy air. These parameters related the main problems of the determination of how much condensed water ultimately falls out as rain need further improvement.

Some validations of this representation of convection are underway and will be reported in the near future (Emanuel). We also hope in near future the improvement will be incorporated into the scheme to give better prediction for practical applications.

APPENDIX A. SUBROUTINE ESAT

This subroutine computes the saturation vapor pressure with respect to water or ice at a given temperature. The saturation vapor pressure e_s is given by

$$e_s = [a_0+a_1T+a_2T^2+a_3T^3+a_4T^4+a_5T^5+a_6T^6] \times 10^3 \quad \text{for } T > -49^{\circ}C, \text{ and}$$

$$e_s = [b_0+b_1T1+b_2T1^2+b_3T1^3+b_4T1^4+b_5T1^5+b_6T1^6] \quad \text{for } T \leq -49^{\circ}C,$$

where $T1 = T-273.15^{\circ}$

$a_0 = 6.98356082665X10^3$ $\quad b_0 = 4.866786841$

$a_1 = -1.88882598347X10^2$ $\quad b_1 = 3.152625546X10^{-1}$

$a_2 = 2.13316439481$ $\quad b_2 = 8.640188586X10^{-3}$

$a_3 = -1.28849310278X10^{-2}$ $\quad b_3 = 1.279669658X10^{-4}$

$a_4 = 4.39338663699X10^{-5}$ $\quad b_4 = 1.077955914X10^{-6}$

$a_5 = -8.02373897717X10^{-8}$ $\quad b_5 = 4.886796102X10^{-9}$

$a_6 = 6.136820929X10^{-11}$ $\quad b_6 = 9.296950850X10^{-12}$

APPENDIX B. THERMODYNAMIC CONSTANTS AND EQUATIONS

$C_{PD} = 1005.7 \quad J \cdot Kg^{-1} \cdot K^{-1}$

specific heat of dry air at constant pressure

$C_{PV} = 1870.0 \quad J \cdot Kg^{-1} \cdot K^{-1}$

specific heat of water vapor

$C_L = 4190.0 \quad J \cdot Kg^{-1} \cdot K^{-1}$

specific heat of liquid vapor

$R_V = 461.5 \quad J \cdot Kg^{-1} \cdot K^{-1}$

gas constant for water vapor

$R_D = 287.04 \quad J \cdot Kg^{-1} \cdot K^{-1}$

gas constant for dry air

$L_v = 2.50 \times 10^6 \ J \cdot Kg^{-1}$
latent heat of vaporization at 0°C.

$$\theta = T\left(\frac{P_0}{P}\right)^{R/C_p}$$ potential temperature

where $P_0 = 1000$ mb $\qquad R/C_p = \dfrac{R_D + R \times R_V}{C_{PD} + R \times C_{PV}}$

$RH = R/RS$ relative humidity

where R is mixing ratio and RS is saturation mixing ratio.

REFERENCES

Anthes, R. A., 1977: A cumulus parameterization scheme utilizing a one-dimensional cloud model. *Mon. Wea. Rev.*, **105**, 270-286.

Arakawa, A., and W. H. Schubert, 1974: Interaction of a cumulus cloud ensemble with the large-scale environment. Part I. *J. Atmos. Sci.*, **31**, 674-701.

Betts, A. K., 1986: A new convective adjustment scheme. Part I: Observational and theoretical basis. *Quart. J. Roy. Meteor. Soc.*, **112**, 677-691.

Betts, A. K., and B. A. Albrecht, 1987: Conserved variable analysis of the convective boundary layer thermodynamic structure over the tropical oceans. *J. Atmos. Sci.*, **44**, 83-99.

Elsberry, R. L., 1990: International experiments to study tropical cyclones in the western North Pacific. *Bull. Amer. Meteor. Soc.*, **71**, 1305-1316.

Elsberry, R. L., B.C. Diehl, J.C.-L. Chan, P.A. Harr, G.J. Holland, M. Lander, T. Neta, and D. Thom, 1990: ONR Tropical Cyclone Motion Research Initiative: Field experiment summary. Technical Report NPS MR-91-001 Naval Postgraduate School, Monterey, CA 93943, 106 pp.

Elsberry, R. L., W. M. Frank, G. J. Holland, J. D. Jarrell and R. L. Southern, 1987: *A global view of tropical cyclones*. Office of Naval Research Marine Meteorology Program. Naval Postgraduate School, Monterey, CA 93943.

Emanuel, K. A., 1981: A similarity theory for unsaturated downdrafts within clouds. *J. Atmos. Sci.*, **38**, 1541-1557.

Emanuel, K. A., 1989: The finite-amplitude nature of tropical cyclogenesis. *J. Atmos. Sci.*, **46**, 3431-3456.

Emanuel, K. A., 1991: A scheme for representing cumulus convection in large-scale models. *J. Atmos. Sci.*, **48**, 2313-2335.

Harr, P. A., T. Neta and R. L. Elsberry, 1991: ONR Tropical Cyclone Motion Research Initiative: Data users guide to observations. Technical Report NPS MR-91-006, Naval Postgraduate School, Monterey, CA 93943.

Houze, R. A., Jr., 1989: Observed structure of mesoscale convective systems and implications for large-scale heating. *Quart. J. Roy. Meteor. Soc.*, **115**, 425-462.

Kuo, H.-L., 1965: On formation and intensification of tropical cyclones through latent heat release by cumulus convection. *J. Atmos. Sci.*, **22**, 40-63.

Kuo, H.-L., 1974: Further studies of the parameterization of the influence of cumulus convection on large-scale flow. *J. Atmos. Sci.*, **31**, 1232-1240.

Ooyama, K., 1971: A theory on parameterization of cumulus convection. *J. Meteor. Soc. Japan.* **49**, (Special issue), 744-756.

Paluch, I. R., 1979: The entrainment mechanism in Colorado cumuli. *J. Atmos. Sci.*, **36**, 2462-2478.

Raga, G. B., J. B. Jensen and M. B. Baker, 1990: Characteristics of cumulus cloud bands off the coast of Hawaii. *J. Atmos. Sci.*, **47**, 338-355.

Raymond, D. J., and M. H. Wilkening, 1982: Flow and mixing in New Mexico mountain cumuli. *J. Atmos. Sci.*, **39**, 2211-2228.

Raymond, D. J., and A. M. Blyth, 1986: A stochastic model for nonprecipitating cumulus clouds. *J. Atmos. Sci.*, **43**, 2708-2718.

Taylor, G. R., and M. B. Baker, 1991: Entrainment and detrainment in cumulus clouds. *J. Atmos. Sci.*, **48**, 112-121.

Warner, J., 1970: On steady state one-dimensional models of cumulus convection. *J. Atmos. Sci.*, **27**, 1035-1040.

Warner, J., and P. Squires, 1958: Liquid water content and the adiabatic model of cumulus development. *Tellus*, **10**, 390-394.

INITIAL DISTRIBUTION LIST

Defense Technical Information Center Cameron Station Alexandria, VA 22304	2
Dudley Knox Library Code 0142 Naval Postgraduate School Monterey, CA 93943	2
Department of Meteorology Naval Postgraduate School Monterey, CA 93943	1
Dr. Russell L. Elsberry Code MR/Es Naval Postgraduate School Monterey, CA 93943	1
Dr. Pe-Cheng Chu Code OC/Cu Naval Postgraduate School Monterey, CA 93943	1
LCDR Yin Tzyh-Chyang 5-3, NO. 63, Chung Hwa 1st Rd. Kaohsiung, Taiwan, R. O. C.	3

Thesis
Y49 Yin
c.1 Tests of a convective
cloud model with soundings
during the TCM-90 field
experiment.